IMPACT OF TIBETAN LAND SURFACE CONDITIONS ON ASAR BACKSCATTERING
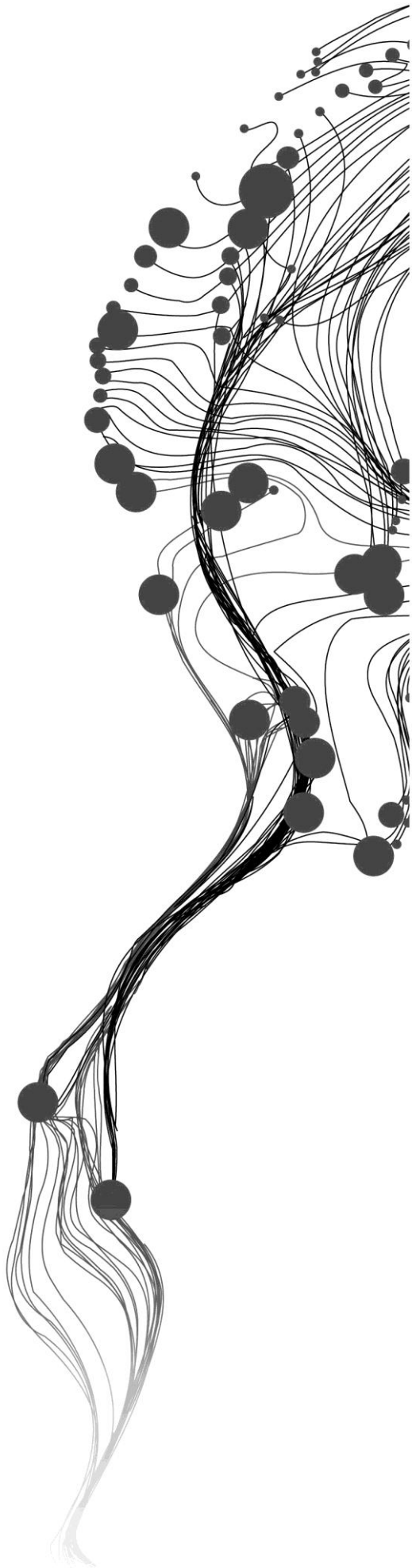
SEIFE GEDAMU ASNAKE
February, 2011

SUPERVISORS:

Dr. Ir. Rogier van der Velde
Dr. Zoltán Vekerdy

IMPACT OF TIBETAN LAND SURFACE CONDITIONS ON ASAR BACKSCATTERING

SEIFE GEDAMU ASNAKE

Enschede, The Netherlands, February, 2011

Thesis submitted to the Faculty of Geo-Information Science and Earth Observation of the University of Twente in partial fulfilment of the requirements for the degree of Master of Science in Geo-information Science and Earth Observation.
Specialization: Water Resources and Environmental Management

SUPERVISORS:
Dr. Ir. Rogier van der Velde
Dr. Zoltàn Vekerdy

THESIS ASSESSMENT BOARD:
 Prof. Dr. Z. Su (Chair)
 Prof. Dr. Ir. N.C. van de Giesen (External Examiner, Faculty of Civil Engineering and Geosciences - Delft University)

ABSTRACT

Tibetan plateau is the highest plateau in the world and is characterized by mountainous ranges with the average altitude of more than 6000 meter above sea level. Understanding the land surface-atmosphere interactions on Tibetan plateau is critical to better understand the Asian monsoon system and its link to climate change. This study analyse the response of ASAR WSM backscattering in relation to variations in land surface conditions over Tibetan plateau. The land surface states analysed are soil moisture, soil temperature and vegetation changes. The study focuses on Maqu Catchment which is located in the north-eastern edge of Tibetan plateau. Grassland, wetland, and hill slope geographical regions are representative for the study area. Soil moisture and temperature data collected in the period 2008 to 2009 were obtained from soil moisture measurement network installed in Maqu catchment and precipitation data were collected from Maqu meteorological station. SPOT NDVI product was used to analyse the effect of vegetation on ASAR WSM backscattering. ASAR WSM images have been processed using ENVI and IDL programming. The average ASAR WSM backscattering coefficient from homogeneous areas (3×3 pixel square window) surrounding each soil moisture stations were extracted. The temporal ASAR WSM backscattering signature over grassland wetland and hill slope shows similar trend. The lowest backscattering value was found during winter season. The backscattering increases from winter to summer season when the monsoon sets in and frozen soil water melts. Compared to the grassland and hill slope stations, wetland stations show the lowest backscattering signature during winter time. The seasonal variation, particularly, the frozen condition affects the backscattering. The spatial profile at three transects across yellow river during winter season shows high backscattering signature. High correlation exists between soil moisture and ASAR backscattering (R^2 up to 0.88) and this suggests the backscattering response was sensitive to soil moisture. Towards the summer the area vegetation cover (NDVI) increases gradually and reaches maximum when the rainfall is at the peak intensity. The soil moisture and soil temperature declines during winter time. The backscattering coefficient increases in 10 dB towards summer season. The increase in backscattering signature follows the monsoon rainfall, the soil moisture state and vegetation biomass change. The correlation between the NDVI of grassland stations versus the mean NDVI was high (R^2 greater than 0.9) and the root mean square difference (RMSD) and bias was low (approximately 0.05). The high coefficient of determination (R^2) and low RMSD and bias suggest the homogeneity of the grassland cover. The correlation between backscattering and NDVI in all grassland, wetland and hill slope sites was low. This shows the effect of vegetation on backscattering was minimum compared to soil moisture. The result of this study show that ASAR WSM data can be used to monitor variations in land surface conditions on Tibetan grassland, wetland and hill slope areas, particularly sites with homogeneous grass cover. In addition, ASAR WSM observation could be a good choice for estimating soil moisture and monitoring the effect of seasonal climatic variation on land surface state such as freezing/thawing condition for hydrological modelling and integrated watershed management.

Keywords: ASAR WSM, backscattering, soil moisture, soil temperature, NDVI, grassland, wetland, hill slope, ENVI/IDL

ACKNOWLEDGEMENTS

TABLE OF CONTENTS

LIST OF FIGURES

LIST OF TABLES

1.   INTRODUCTION

1.1.   Background

The Tibetan plateau is the highest plateau in the world, undulating around 3500-4500m and boarded by mountainous ranges with the average altitude of more than 6000 meter above sea level. Understanding the land surface-atmosphere interactions on the Tibetan plateau, the so-called roof of the world, is critical to better understand the Asian monsoon system and its link to climate change (Cui et al., 2006). Soil moisture is a key component in coupling water and energy fluxes at the interface between land surface and atmosphere. Soil moisture at the land surface affects the infiltration and thus the partitioning of precipitation into runoff and subsurface water storage. The uppermost soil layer influences surface energy balance by affecting partitioning of solar radiation in to sensible and latent heat flux. As a result, considerable effort has been devoted to the retrieval of spatially distributed soil moisture. Low frequency (C-band and lower) Synthetic Aperture Radar (SAR) remote sensing has shown to provide data sets that can be used for high resolution soil moisture mapping (Baup et al., 2007; Paloscia et al., 2008; Thoma et al., 2008; Zhang et al., 2009).

Advanced Synthetic Aperture Radar is currently operational on the European Environmental Satellite (EnviSat) at 5.3 GHz frequency. The ASAR instrument can operate in five modes: Wave mode (WM), Image mode (IM), Alternating Polarization mode, Wide Swath mode (WSM) and Global Monitoring mode (GM) . The ASAR sensor transmits electromagnetic signal to the surface and receives the returned signal from the target. The backscattered energy from the target is dependent upon several factors such as surface roughness, geometry, and orientation of the target, complex dielectric property and incident wave property. Furthermore, sensor configuration (frequency, polarization, view angle) also affects backscattering signal. These factors influence the returned signal by affecting the amplitude of the backscattering coefficient.

The backscattering coefficient depends on the dielectric property of the target. At a microwave frequency, the surface dielectric properties are strongly affected by land surface conditions such as surface soil moisture and vegetation cover. Analysis of the measured radar backscattering coefficients can provide valuable information on the surface soil moisture content, roughness characteristics of the soil surface, and the vegetation cover. Previous studies investigated SAR observation for its potential to observe changes in land surface states such as soil moisture (Loew et al., 2006; Rahman et al., 2008; Su, 1997; Van der Velde et al., 2008), vegetation cover (Minchella et al., 2009; Tsan et al., 1984; Ulaby, 1981) and frozen conditions (Rignot & Way, 1994; Wegmüller, 1990).

Quantifying backscattering contribution from soil surface and vegetation over large area needs complex parameterization. Estimating scattering from vegetation is difficult because of its complex vegetation morphology. However, analysing the change in the land surface conditions (such as soil moisture, soil temperature, vegetation density) increase the understanding to interpret the measured backscattering coefficient.

This study analyses HH and VV polarized ASAR WSM observations to characterize the impact of Tibetan land surface conditions on backscattering signatures. Grassland, wetland, and hill slope geographical regions selected to represent the study area. The land surface states analysed in this study are soil moisture, soil temperature and vegetation. There are 20 soil moisture measurement network stations installed in

Maqu catchment. The soil moisture and soil temperature record of these stations and SPOT Normalized Difference Vegetation Index (NDVI) product are utilized to study the impact of vegetation on ASAR WSM temporal backscattering variability.

1.2. Problem statement

Scattering of the microwaves signal depends on several factors such as surface roughness, geometry, orientation of the target and complex dielectric property for known sensor configuration (view angle, polarization, wave length and frequency). Describing the scattering contribution from each factor mathematically is difficult because of the irregular geometry of surface and vegetation under natural conditions.

Modelling scattering using either physically based or semi-empirical approaches needs rigorous parameterization of vegetation morphology including vegetation size, shape, and water content and also 2-dimensional surface height variation and it is difficult to get all the necessary parameter at large scale.

Previous studies have shown that microwave backscattering is sensitive to soil moisture variations as well as surface roughness and vegetation (Rahman et al., 2008). The land surface conditions especially soil moisture, and vegetation determines the backscattering towards the sensor. Inversely, analysing the temporal variation of the total backscattering measurement provides information on land surface condition, particularly soil moisture and vegetation variation.

1.3. Research objective

The primary objective of this study is to evaluate the temporal and spatial variability of ASAR WSM backscattering signatures observed over the Maqu Study area as a function of land surface variables (particularly soil moisture, soil temperature and vegetation cover and to investigate the sensitivity of these relationships to the polarization.

Specific objective of this study are
- To define the temporal ASAR WSM backscattering variability over grassland, wetland and hill slope sites
- To identify the effect of soil moisture and vegetation on ASAR WSM backscattering
- To identify the effect frozen condition on ASAR WSM backscattering

1.4. Research questions

From the above objective the following research questions follow:
1. How change in soil moisture, vegetation cover, and topography affect ASAR WSM backscattering?
2. How the frozen condition affect the ASAR backscattering?
3. What is the effect of soil moisture on ASAR WSM backscattering?
4. What is the effect of vegetation cover on ASAR WSM backscattering?

1.5.   Hypothesis

1. In the Maqu area grassland vegetation has a small contribution to ASAR backscattering, which is, as such, expected to be dominated by surface scattering and sensitive to soil moisture.
2. The relationship between soil moisture and ASAR backscattering signal can be approximated by linear relationship.

1.6.   Thesis structure

This thesis is organized in six Chapters. The first Chapter gives brief introduction, problem statement, research objective and the research questions followed by hypothesis of the study. Chapter two of this thesis discusses the theoretical background of the study supported by a review of previous literature on the study area and related investigations. Chapter three describes the study area and field data collection. The technique of image processing and the method to conduct this study is discussed in Chapter four. Chapter five briefly discuss the result and discussion of this thesis. In the last chapter, Chapter six, the conclusions of the study and recommendations for further study is presented.

2. THEORETICAL BACKGROUND

2.1. Background

Previous studies showed that microwave remote sensing has the capacity to estimate surface soil moisture in reasonable accuracy (Baup et al., 2007; Joseph et al., 2008; Loew et al., 2006; Low et al., 2005; Schmugge & Thomas, 1983; Su, 1997; Ulaby et al., 1996; Wang et al., 1989; Zhang et al., 2009; Zribi et al., 2003). Currently, various satellites carrying microwave sensor are in orbit. Space-borne passive microwave systems possess the advantage of high revisit time; however, the spatial resolution of passive microwave remote sensing is too coarse for applications at regional scale. However, active microwave remote sensing from satellites has the capacity to provide high spatial resolution with fair temporal resolution of 4 to 6 days. This makes active microwave remote sensing supportive for application at the regional scale for watershed management and hydrological studies.

The interest of studying soil moisture from satellite significantly increased, with availability low frequency microwave sensors, in the past two decades. ERS 1 and 2 launched on 19th February and 7th February 1990, respectively by from European Space Agency (ESA). Both ERS sensors provide backscatter measurements in C-band and 5.33 GHz frequency range at VV-Polarization and a nominal incidence angle of 23 degrees. Canadian Space Agency (CSA) launched Radarsat 1 and 2 on 4th November, 1995 and 14th December, 2007. Japanese Space Agency (JAXA) launched the Japanese Earth Radar Satellite (JERS-1). The JERS-1 sensor is a L-band (1.4 GHz) HH-polarized radar at nominal incidence angle of 39 degrees. The National Aeronautics and Space Agency (NASA) launched the Shuttle Imaging Radar SIR-C/X-SAR (C and X band) and TRMM microwave imager (TMI) at 10.66 GHz. European Space Agency (ESA) also launched ENVISAT on 01 March, 2002, and SMOS on 02 November, 2009.

2.2. Why active microwave remote sensing?

The different part of electromagnetic spectrum provides specific information on the target. The microwave remote sensing operates at longer wave length (1 cm -30 cm). Microwave remote sensing has an advantage than optical remote sensing because microwaves can penetrate haze, light rain and snow, clouds and smoke, these waves are good for viewing the Earth from space.

Passive microwave technique uses energy emitted from earth surface where as active microwave transmit and they receive their own energy and therefore it is possible to get day and night measurement in all kinds of weather. In addition, the spatial resolution of passive microwave remote sensing is very coarse (up to 10th of kilometre) where as active microwave observation provides high resolution data set (up to 25th meter) which makes active microwave remote sensing suitable for studies at catchment scale.

2.3. Surface roughness and dielectric property

The surface roughness affects the returned microwave signal. Smooth surface like water scatters the incoming microwave signal away from the sensor and results in low backscattering. Whereas rough surfaces like soil scatter the transmitted microwave signal in every direction including the sensor and results high backscattering measured by the sensor.

According to the Rayleigh criterion, a surface is considered to be rough if the mean height of the surface variation should be greater than the ratio of the wave length by eight time cosine of the incidence angle. (European Space Agency, 2010)

$$h < \frac{\lambda}{8 * \cos \theta}$$
<div align="right">Equation 2-1</div>

Where; h is the mean surface variation and θ is the incidence angle and λ is the wavelength.

The backscattering component from soil surface can be approximated by using the root mean square height variation and autocorrelation length. The autocorrelation length function is often defined as Gaussian or exponential function. This approximation is based on the assumption that the surface is isotropic and the change in roughness through time is small.

Dielectric constant (εr) of a material is the ratio of permittivity of the material (ε) to permittivity of free space (ε0). If the medium absorbs energy from the electromagnetic wave propagating through it, the dielectric constant is represented by complex number. The complex dielectric constant εr is given as:

$$\varepsilon_r = \varepsilon' - j\,\varepsilon''$$
<div align="right">Equation 2-2</div>

where, ε' is the permittivity of the material, the real component defining the velocity and wavelength of the refracted wave in the material; and ε'' is the imaginary part of the dielectric constant, the dielectric loss factor, expressing energy lost through absorption of the wave in the medium. Dobson et al, (1985) showed that the increase in the volumetric soil moisture content causes the real part of the dielectric constant to increase more than the imaginary part of the dielectric constant.

Soil is a heterogeneous mixture of soil mineral, water, air and its dielectric property depends on soil texture, water content and salinity. As the amount of moisture in the soil increases the dielectric constant reaches the value of 20 or more.(Schmugge & Thomas, 1983)

2.4.   Backscattering coefficient and Land surface conditons

The semi empirical water–cloud model first developed by Attema and Ulaby (1978) expressed the backscattering coefficient as a sum of contribution from vegetation volume scattering, surface scattering by the underlying soil layer, and multiple interaction between the vegetation and the soil underneath.

$$\sigma^0 = \sigma^0_{veg} + \sigma^0_{veg+soil} + \tau^2\,\sigma^0_{soil}$$
<div align="right">Equation 2-3</div>

The second term vegetation–soil interactions are neglected in the water–cloud model. Therefore, the above expression can be simplified as;

$$\sigma^0 = \sigma^0_{veg} + \tau^2\,\sigma^0_{soil}$$
<div align="right">Equation 2-4</div>

The second term which is scattering from underlying soil is attenuated by a vegetation cover factor τ^2. It is the two-way vegetation transmisivity expressed by;

$$\tau^2 = \exp(-2Bm_v \sec\theta)$$
<div style="text-align: right">Equation 2-5</div>

And

$$\sigma_{veg}^0 = Am_v(1 - \tau^2)$$
<div style="text-align: right">Equation 2-6</div>

Where, τ^2 is the two-way vegetation transmisivity, θ is incidence angle and m_v is the vegetation water content (kg/m³). A and B are parameters that depend on the canopy type. A is the maximum allowable attenuation from the vegetation canopy. A can be interpreted as a vegetation density parameter (0 for bare soil, a very high value for evergreen forests (Bindlish & Barros, 2001).

Vander Velde et al. (2008) studied the impact of soil moisture dynamics on the mean ASAR WSM backscattering signatures and its spatial variability on Naqu region (also on Tibetan plateau) at four different study areas which were covered by a mixture of grassland and wetland. In this study he concluded that, the impact of the soil moisture dynamics during monsoon and winter periods on the backscattering signature and its spatial variability is consistently observed on all four selected spatial domains. His findings are confirmed through a comparison of the mean backscattering and standard deviation with in-situ soil moisture measurements at a single station.

The backscattering coefficient from ASAR AP mode 30 meter spatial resolution has been modelled to estimate soil moisture estimation over loss plateau in China (Zhang et al., 2009). In addition, ASAR observation has been used to estimate soil moisture in different region (Baup et al., 2007; Loew et al., 2006; Low et al., 2005; Paloscia et al., 2008; Rahman et al., 2008). Therefore, the land surface conditions, especially soil moisture variation, vegetation cover and surface roughness have major impact on the backscattering signal.

Analysing the backscattering signature would improve the understating of change in land surface conditions primarily, soil moisture, vegetation cover and surface roughness. However, the temporal change of surface roughness is insignificant under natural condition unless there is a change in surface condition (e.g. agricultural practice such as ploughing). Therefore, the temporal backscattering signature would be dependent on soil moisture and vegetation cover.

ASAR WSM backscattering observation which has fairly high spatial and temporal resolution could be used to study the change in the land surface conditions (such as soil moisture and vegetation cover) and could also be used to identify the impact of soil moisture and vegetation on the backscattering signal.

3. STUDY AREA AND FIELD WORK

3.1. Description of the study area

Maqu is located at the north-eastern edge of the Tibetan Plateau (33°30'-34°15'N, 101°38'-102°45'E), in the Gansu province, China. The region is situated at an elevation ranges between 3430 m and 3750 m above mean sea level. Yellow river, the second longest river in China, flows through Maqu Catchment. The study area consists of 20 soil moisture monitoring stations.
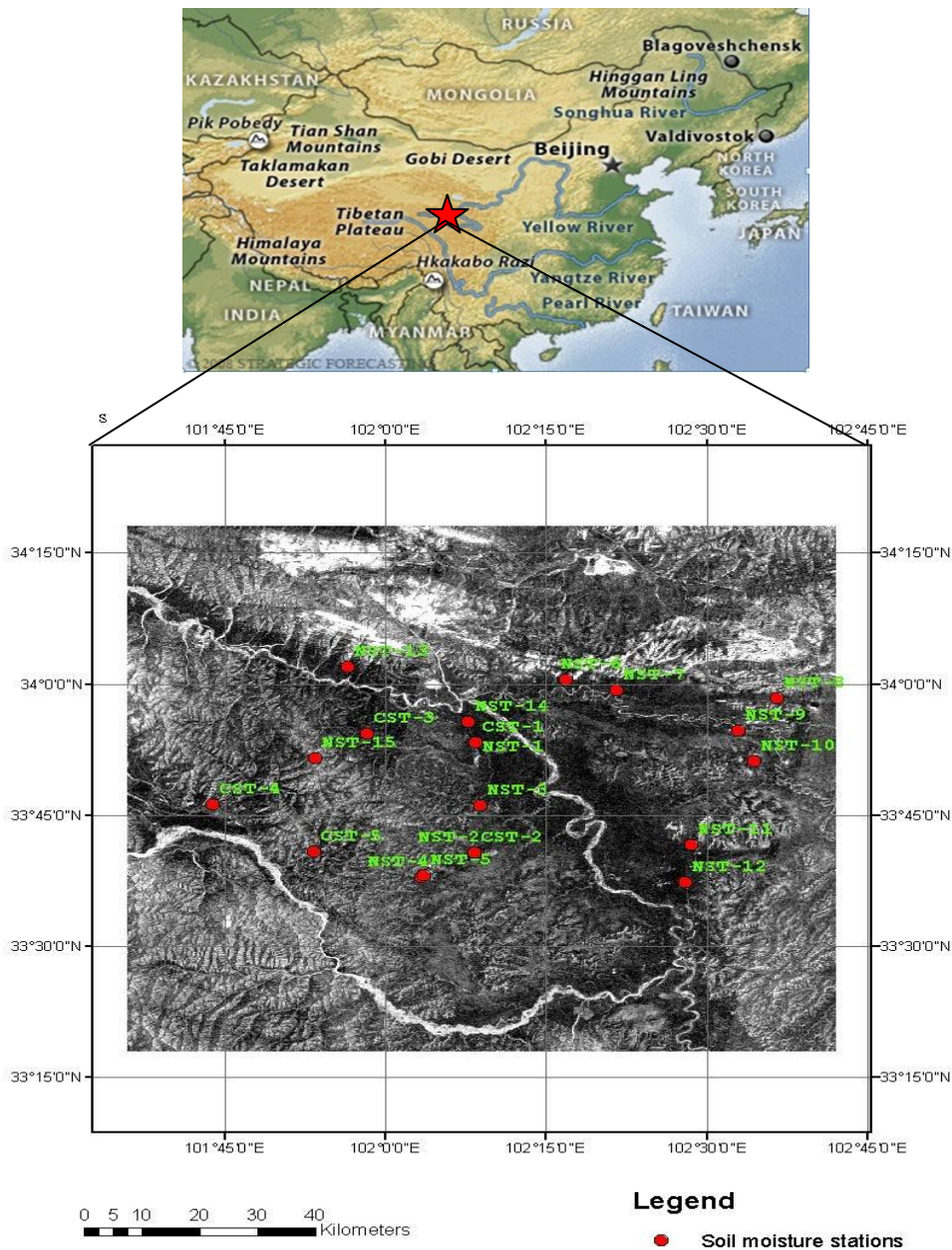
Figure 3-1 Location of Maqu soil moisture monitoring network (Red point) over Maqu study area

Source: http://www.map-of-china.org/ (Accessed date Thursday, December 16, 2010)
The climate of the study area is cold and wet with the features that the mean annual precipitation is 597.1 mm and the mean annual temperature is 1.40 °C. The temperature drops below freezing point during

winter time from December through February. The precipitation in the study area is influenced by Asian monsoon with rainy summer and cold winter. The rainy season starts from May through September and reaches its peak intensity during August. According to Koeppen Classification System, the climate at Maqu study area is defined as wet and cold, with dry winters and rainy summers due to Asian monsoon. (Dante et al., 2009)

The land cover of the area consists of mainly homogeneous short grassland, wetlands, degraded grassland, and bare areas. Wetlands, with typically organic soils, characterize a large part of the valleys. The topography of the study area composed of the valleys of the yellow river and its tributaries; and rolling terrain of hills and mountains and the whole regions is characterized by a uniform cover of short grassland used for grazing.

Figure 3-2 View of Maqu study area

The soil texture of the study area is primarily silt-loam and in some areas sandy loam can be found. Silt loam is the dominate soil texture which is found on all NST stations except NST-09 which has sandy loam soil texture.

The average organic matter content of stations located on grass with silt loam soil texture land is 27.54 g/kg. Howe ever, wetland stations, NST-04 and NST-11 has high amount of organic matter content of 229.07 g/kg and 135.74 g/kg, respectively. The Maqu wetland is an important source of water for Yellow river.

3.2. Soil moisture station network

In a cooperation between ITC and Cold and Arid Regions Environment and Engineering Research Institute, Chinese Academy of Sciences (CAREERI) a network of 20 soil moisture measurement stations has been installed in the region where the Heihe confluences with the Yellow River. The soil moisture network installed in Maqu catchment measures soil moisture and temperature at depth ranging from 5 cm to 80 cm from July, 2008 onwards. The network covers an area of approximately 40 by 80 km.   Each station consists of one Em50 ECH2O data logger, which records the soil moisture and temperature collected by two to five EC-TM ECH2O probes. The EC-TM ECH2O probe consists of three flat prongs, 5.2 cm long. Using an oscillator running at 70 MHz oscillating wave, the probes measures the dielectric permittivity of soil to determine the water content and a thermal sensor of the soil surrounding the prong

Table 3-1 List of measurement uncertainty for soil moisture and temperature (Decagon Devices, 2007)

EC-TM ECH2O probe	Volumetric Water content (VWC)	Temperature (^{0}C)
Range	0 - 100 %	- 40 - 50
Resolution	1 %	0.1
Accuracy	± 3 %	± 1

The dielectric permittivity is then converted to volumetric soil moisture according to a standard calibration equation. EC-TM ECH2O probe is valid for all fine textured mineral soils with an accuracy of approximately ± 3%. The EC-TM ECH2O probe were tested in four different types of soils (Sand, sandy loam, silt loam, and clay) and the calibration equation generated from these tests is shown below (Decagon Devices, 2007)

$$\theta = 1.087 * 10^{-3} * Raw - 0.629$$ <div align="right">Equation 3-1</div>

Where θ Volumetric is water content, and Raw is output of probe measurement. However, soil specific calibration increases accuracy from 1% up to 2 % in VWC.
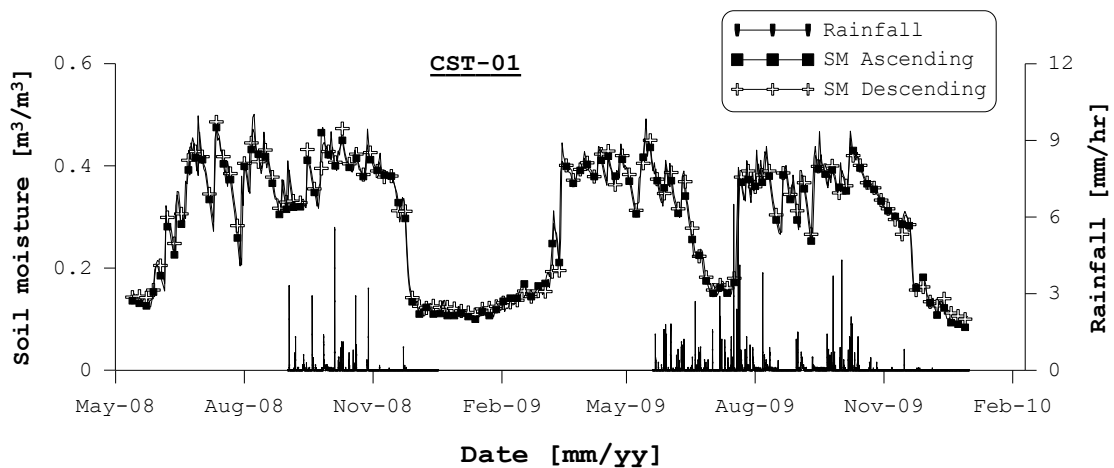
Figure 3-3 Soil moisture trend at station CST-01 (close to Maqu metrological station) and rainfall

Figure 3-3 shows the soil moisture trend over CST-01 station and the rainfall record from metrological station next to it. The soil moisture during winter season is low (< 0.2 m³/m³) and remains stable until the end of winter season. The soil moisture increases towards summer season when the area receives rainfall.

3.3.   Field work data collection

Data about soil moisture, soil temperature and precipitation of the area have been collected during the field work campaign that was held for two weeks, from 11 September to 25 September, 2011. The soil moisture and temperature measurements which are taken every 15 minute interval were downloaded from all stations. ASAR WSM (C-band 5.3 and GHz frequency) signal can penetrate the top soil layer, a few centimetre depths (up to 5 cm). The soil moisture and temperature measurement at this soil profile (5 cm) is used for further analysis. The rainfall was measured at Maqu metrological station near to station CST-01 at 30 minute interval. The data has been provided by Cold and Arid Regions Environment and Engineering Research Institute, Chinese Academy of Sciences (CAREERI).

The geographical coordinate of all soil moisture station were registered at the time of installation. With the help of GPS and each station coordinate (latitude and longitude), it was possible to locate the buried logger for downloading the data.

Soil moisture around the soil moisture stations were measured using Theta probe in two transect crossing the grassland and wetland a station and along the contour on hill slope station. The measurements were taken at same time while downloading the soil moisture from the logger. The last Em50 ECH$_2$O logger reading and Theta probe measurement comparison on five stations shows the two measurements are in agreement.   However, in order to investigate how one soil moisture station is representative to the surrounding area and the foot print of ASAR WSM observation, extensive sampling and further analysis needs to be done.

Figure 3-4 Downloading soil moisture and temperature on the field

3.4. Data quality analysis

The soil moisture and temperature of the 20 soil moisture network has been downloaded from Em50 ECH$_2$O data logger. The measurements were taken at every 15 minute interval. In order to evaluate the consistency of the data logger, the soil moisture and temperature record of the first port (5 cm depth) is plotted below from figure 3.5 up to figure 3.7. The soil moisture and temperature record at ENVISAT satellite overpass time at ascending pass (3 a.m.) and descending pass (15 p.m.) has been utilized over three different sites such as grassland, wetland and hill slope [time in GMT]. At the hill slope station (NST-05) a data gap was found from March, 2009 up to Jun 2009.
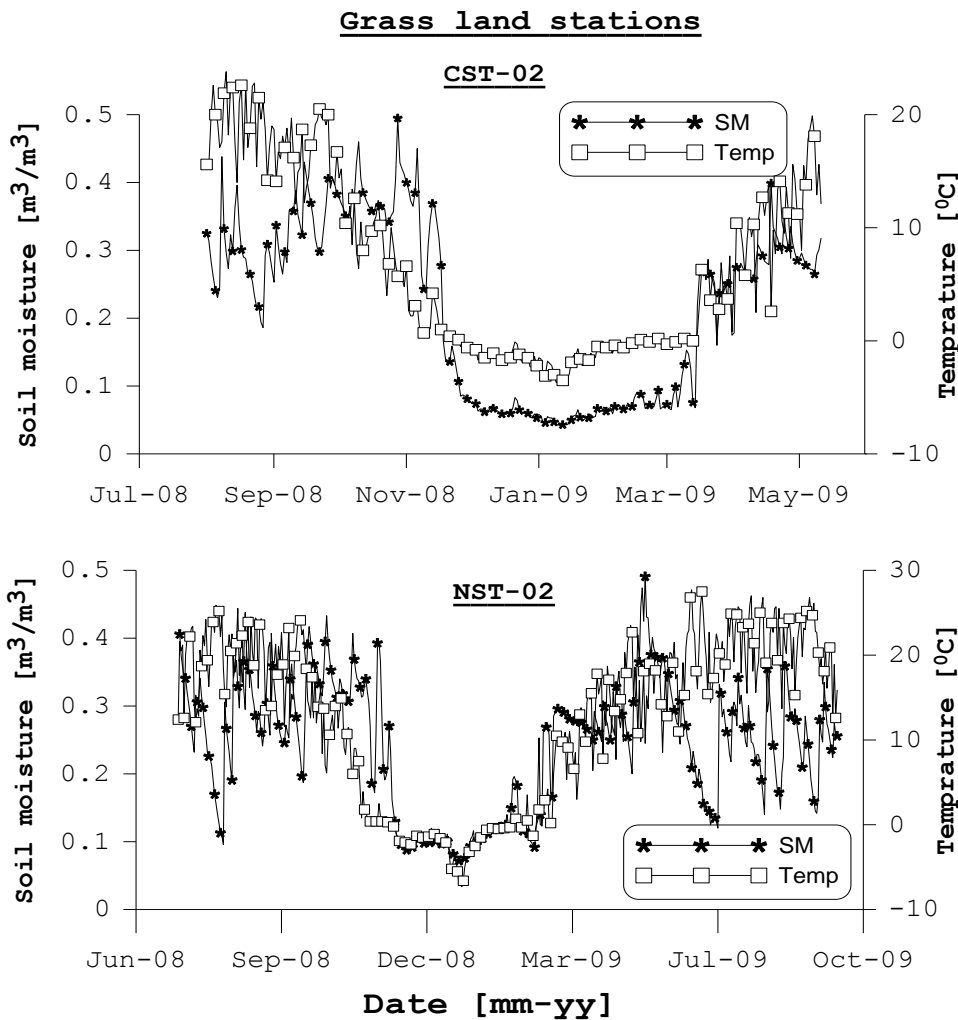
Figure 3-5 In situ soil moisture and temperature trend over grassland at the time of ascending overpass

Figure 3-5 shows the time series of soil moisture and temperature for the top soil layer (at 5 cm depth) over two grassland stations (CST-02 and NST-02) at the time of ascending overpass of the ENVISAT satellite. In the winter period, from December to March the soil temperature drops below freezing point down to -10 ^{0}C. The measured soil moisture in both stations during the winter season was measured as approximately 0.1 (m^3/m^3), although this is not the real value, since the sensors are much less sensitive to the frozen water then the liquid water in the soil.

The wetland stations (NST-04 and NST-11) have high Organic Matter Content of 229.07 g/kg and 135.74 g/kg, respectively. Therefore, the increase in organic matter content in wetland station improves the water holding capacity of the soil for the same soil texture. As shown in Figure 3-6 the soil moisture record on these stations was greater than 0.4 (m³/m³) by volume during summer period (Jun, July, and August) where the area receives high amount of rainfall from Asian monsoon system.

Especially NST-04 has approximately 10 peak soil moisture records. The rainfall variability could be the reason for different recording in the two stations. Since there is only one rain gauge station, it was not possible to observe the soil moisture distribution with spatial rainfall viability. However, the sensors at these wetland stations could also be flooded during the time of measurements.
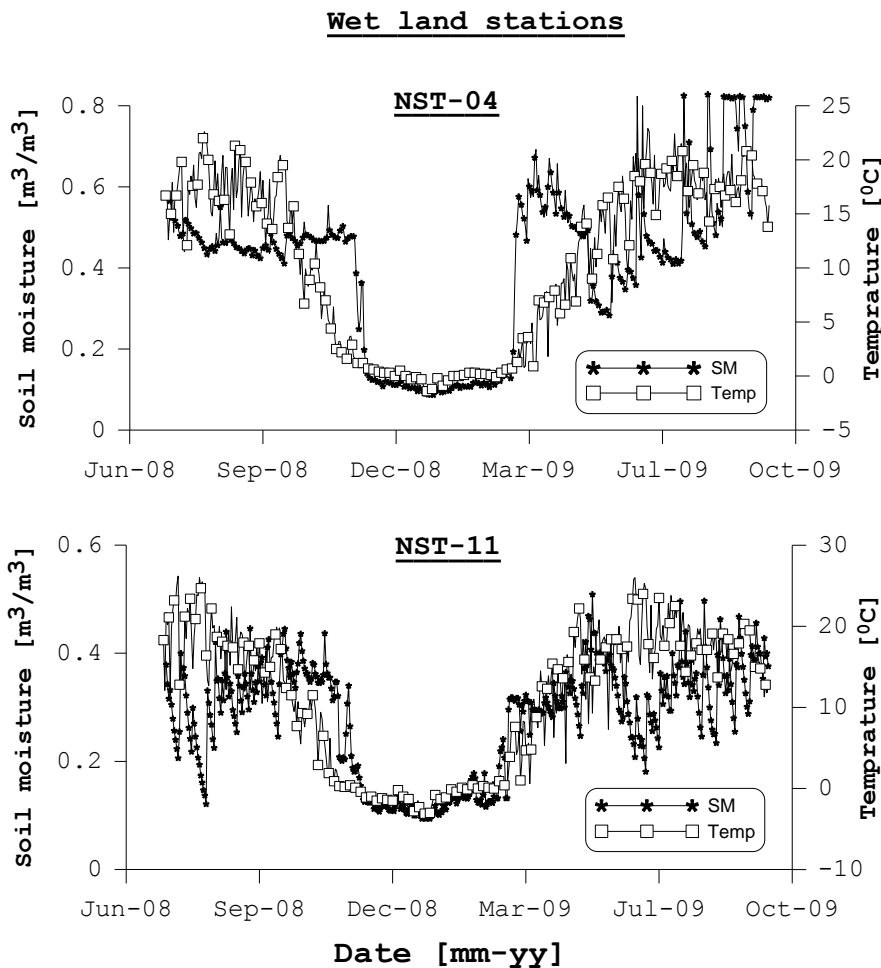
Wet land stations

Figure 3-6 Soil moisture and temperature trend over wetland on ascending pass time

Station NST-05 and NST-15 are the two soil moisture stations installed in hill slope. Howe ever, there was a data gap on soil moisture and temperature record between March and July on station NST-05.

Station NST-15 records high soil moisture up to 0.6 (m³/m³) in the rainy season where as station NST-05 records lower soil moisture content up to 0.4 (m³/m³) The two hill slope station records high soil moisture in summer season up to 0.6 (m³/m3).
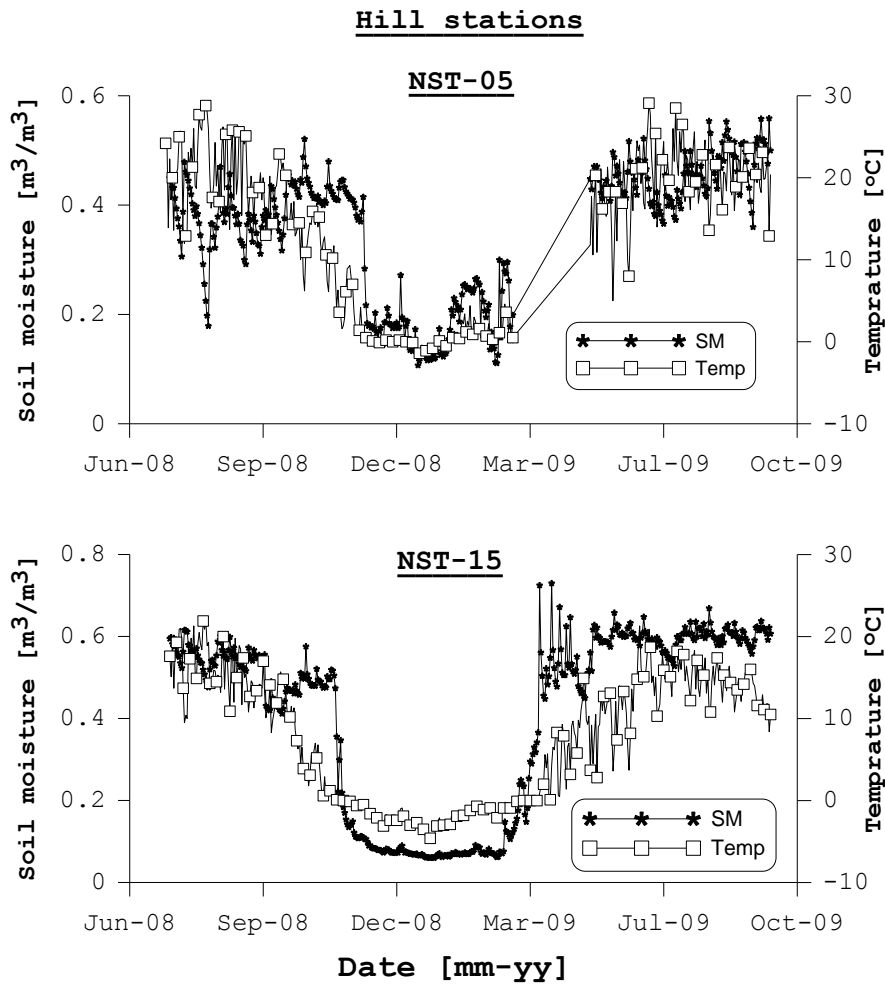
Figure 3-7 Soil moisture and temperature trend over Hill on ascending pass time

Figure 3-7 shows the increasing trend in soil moisture content from winter season (which is considered as dry and cold) towards summer season. The area receives high amount of the rainfall during summer season from Asian monsoon. This leads the soil moisture content over the area to increase during summer.

Generally, figure 3.5 up to figure 3.7 shows the increase in soil moisture trend from May to September and the peak soil moisture records were mostly during August. In all plots, the measured soil moisture and temperature decrease during winter time and the soil becomes very low and the temperature turns to cold. The high soil moisture content during summer shows, as the area receive considerable amount of rainfall.

.

4.   REMOTE SENSING DATA AND METHODS

The main remote sensing data sets of this study are a time series of multi polarized Advanced Synthetic Aperture Radar Wide Swath Mode (ASAR WSM) images and Normalized Difference Vegetation Index (NDVI) product of SPOT VEGETATION observation for the period from January 2008 to December 2009. In addition, ancillary in situ data sets such as soil moisture and temperature have been used for this study.

ASAR WSM observation provides a 400 km by 400 km wide swath image with a spatial resolution of approximately 150 m by 150 m in VV or HH polarisation (EVISAT ASAR Product Handbook, 2002).

Scattering of the microwave signal from the surface depends on several factors such as surface roughness, geometry, and orientation of the target, complex dielectric property and incident wave property. These factors influence the returned signal by affecting the amplitude of the backscattering coefficient. Then the phase and amplitude of the returned backscattering signal is recorded. Backscattering is a ratio between received and transmitted power.

The in situ soil moisture measurement from the twenty soil moisture networks installed in the study area that measures soil moisture at 15 min interval used for correlating the time series of ASAR WSM backscattering coefficient with soil moisture. The VV and HH polarized ASAR WSM (C- band and 5.3 GHz) data were then processed to evaluate the temporal variation of returned backscattering signal in relation to land surface variables. The major softwares used for ASAR WSM image processing are Next Generation SAR Tool box (NEST), ENVI and IDL programming. In this study, GIS software has been used for overlaying the soil moisture stations on the backscattering image and mapping ASAR WSM images and Grapher software has been used for plotting graphs.

To analyse the spatial and temporal ASAR backscattering on the study area, three sites such as grassland, wetland and hill slope were selected. There are 16 grassland stations, 2 wetland stations and 2 hill slope stations. To extract the backscattering response on this study sites, the following IDL codes developed.

1.   To delineate the study area from ASAR images:
2.   To convert DN value to backscattering in power unit [m²/m²] :
3.   To convert backscattering power unit [m²/m²] to decibel unit [dB] :
4.   To normalize the backscattering coefficient to 23 degree incidence angle :
5.   To extract the backscattering at the 20 soil moisture station (study sites) :

SPOT NDVI product has been processed to analyse vegetation cover and its effect on the returned backscattering signal. To compare the spatial and temporal variation of vegetation density and its effect on ASAR backscattering signal the NDVI value is extracted at same location. The following IDL codes were also developed to process and drive the NDVI value at grassland, wetland and hill slope stations.

1.   To convert SPOT DN value to NDVI value:
2.   To extract NDVI value at the 20 soil moisture stations (study sites):

The mean backscattering and NDVI of the 16 grassland station were used for analysis. To further analyse whether the mean backscattering and NDVI represent the grassland station for comparison with wetland and hill slope station, the Root Mean Square Difference (RMSD), Bias and Coefficient of determination

(R²) were calculated. The standard deviation of the backscattering coefficient and NDVI over the grassland station was computed to analyse the deviation from mean.

4.1.   ASAR WSM data set

In this study, the Advanced Synthetic Aperture Radar (EVISAT ASAR Product Handbook) Wide Swath Mode (WSM) with spatial resolution of 150 meter is investigated. ASAR WSM has the ability to collect data over a wider swath of 400 km covering 16 to 43 degrees view angle range with a temporal resolution of 3-4 days. (EVISAT ASAR Product Handbook, 2002).

The ASAR WSM data source for this study was the European Space Agency earth observation multi-mission catalogue and ordering service (Eoli-Sa) ENVISAT ASAR archive. Inputs to search the archived image were the study area centre coordinates (33°30'N, 102°15'E).

The requested ASAR WSM observation was delivered as Ellipsoid Geocoded level 1b product having 75 meter grid spacing, WGS 84 vertical datum and geographic lat/long coordinate system with absolute accuracy of ± 1 dB.

A total of 40 ASAR WSM VV and HH polarized scenes were available in ESA archive that covers the Maqu catchment fully or partially from January, 2008 up to December, 2009 (101.36-102.36 East and 33.18-34.18 West). From the total ASAR WSM data sets, 13 of them were acquired in ascending pass and the rest 27 images were in descending pass.

ASAR acquires measurements at 3:00 a.m. (GMT) in the ascending orbit and 15:00 p.m. (GMT) in the descending orbit. The entire images were collected in Vertical (VV) and horizontal (HH) polarization. The images are listed in the table 1 and 2 of appendix of this thesis.

```
                        ┌─────────────────────┐
                       /   ASAR WSM           /
                      /    data set          /
                     └─────────────────────┘
                              │
              ┌───────────────┴───────────────┐
              ▼                               ▼
      ┌───────────────┐               ┌───────────────┐
      │ Ascending pass│               │ Descending pass│
      └───────────────┘               └───────────────┘
              └───────────────┬───────────────┘
                              ▼
                   ┌─────────────────────┐          ┌─────────────────┐
                   │ Geo registration of │         /  Lat/long  of    /
                   │ ASAR WGS 84 datum   │        /   study area      /
                   │ and geographic      │       └─────────────────┘
                   │ lat/log coordinate  │
                   │ system              │
                   └─────────────────────┘
  ┌──────────────┐         │                              │
 / SRTM   DEM    /         ▼                              │
/  90 m resol.  /  ┌─────────────────────┐◄──────────────┘
└──────────────┘   │ Study area masking  │
        │          │ using ENVI/IDL script│
        │          └─────────────────────┘
        │                   │
        │                   ▼
        └─────────►┌─────────────────────┐        ┌─────────────────┐
                   │ Terrain correction  │       / Calibration      /
                   │ and local incidence │      /  constant, K      /
                   │ angle projection    │     └─────────────────┘
                   └─────────────────────┘              │
                              │                         │
                              ▼                         │
                   ┌─────────────────────┐◄─────────────┘
                   │ DN to backscattering│
                   │ conversion using    │
                   │ ENVI/IDL script     │
                   └─────────────────────┘
  ┌──────────────┐            │
 / 23 degree     /            ▼
/ incidence angle/   ┌─────────────────────┐
└──────────────┘    │ Power to decibel unit│
        │           │ conversion using ENVI/IDL│
        │           └─────────────────────┘
        │                    │
        └─────────►┌─────────────────────┐
                   │ Backscattering      │        ┌─────────────────┐
                   │ normalization using │       / Coordinate  of   /
                   │ ENVI/IDL            │      /  SM stations      /
                   └─────────────────────┘     └─────────────────┘
                              │                         │
                              ▼                         │
                   ┌─────────────────────┐◄─────────────┘
                   │ Backscattering      │
                   │ coefficient         │
                   │ extraction using    │
                   │ ENVI/IDL            │
                   └─────────────────────┘
```
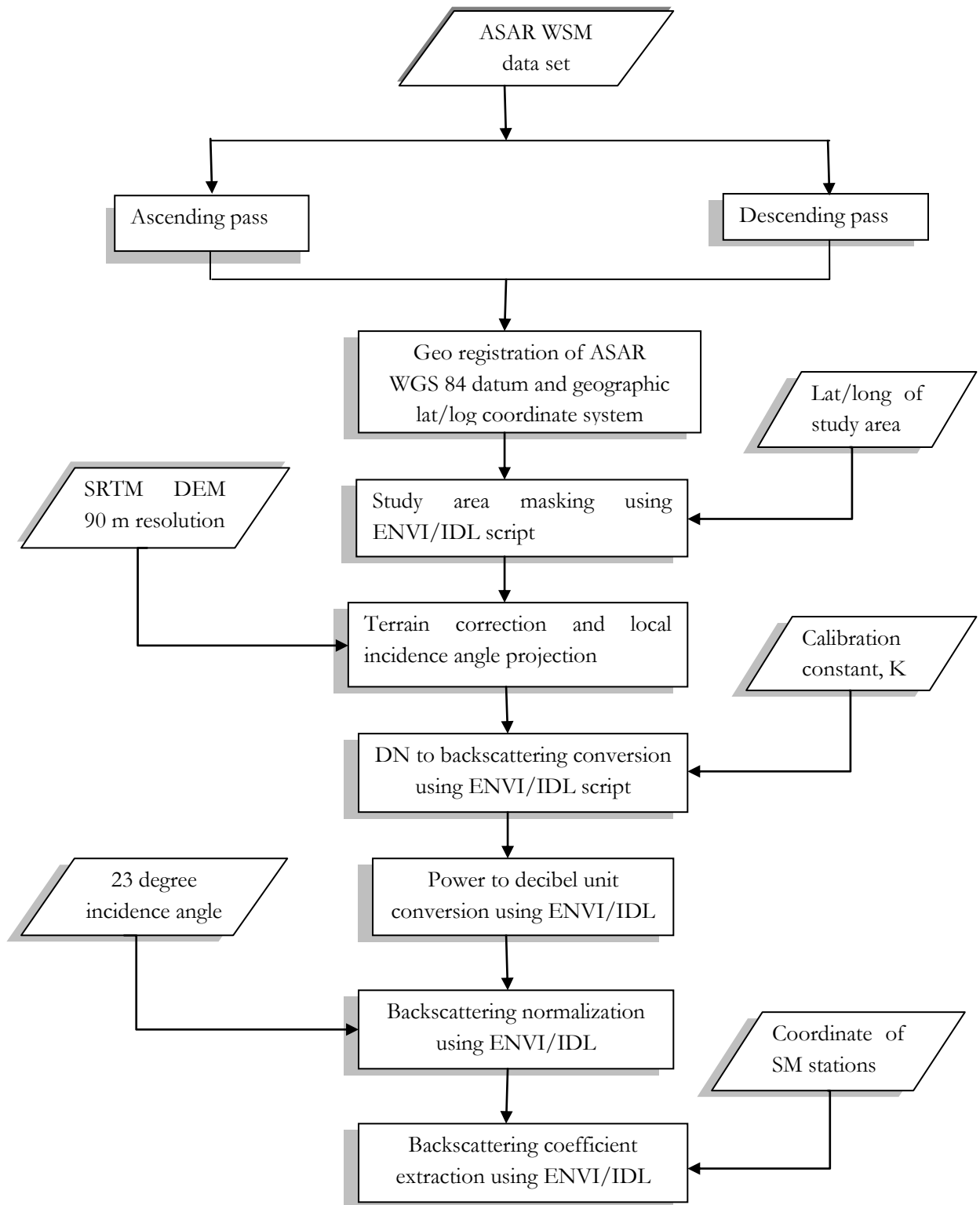
Figure 4-1 Schematization of processing of ASAR WSM images

4.2. Backscattering coefficient derivation

The time series of ASAR images are arranged in ascending and descending passes and processed using NEST (Next generation SAR Toolbox) software from ESA (European Space Agency) and ENVI/IDL program. The backscattering coefficient of ASAR image is calculated with Equation 1 below.

$$\sigma^0 = \frac{(A^2)}{K \sin \alpha_d} \qquad\qquad \text{Equation 4-1}$$

Where σ^0 is the target backscattering coefficient in power unit (m^2/m^2); A is the DN value, α_d is the incidence angle, and K is an external calibration scaling factor.

Then, the target backscattering coefficient (m^2/m^2) for each pixel within the study area were converted to decibel units for analysis using the formula below; (EVISAT ASAR Product Handbook, 2002).

$$\sigma^0 \ (dB) = 10 \log_{10}(\sigma^0) \qquad\qquad \text{Equation 4-2}$$

The ASAR processor on board averages reflected pulses from a number of images and creates a composite multi-look. Therefore, no additional speckle filtering has done because ASAR WSM images were synthesized from 21 look images (3 looks from azimuth and 7 looks in range direction (EVISAT ASAR Product Handbook, 2002).

Due to the topographical variation of the area and tilt of the satellite sensor, distance can be distorted in the ASAR image. Correcting incidence angle for local topography reduces the topographic effect on the backscattering signal so that, so the geometric representation of the image will be as close as possible to the real. Calculation of terrain distortion was carried out by NEST software for local incidence angle correction based on the SRTM DEM by using geographic coordinates with WGS 84 datum.
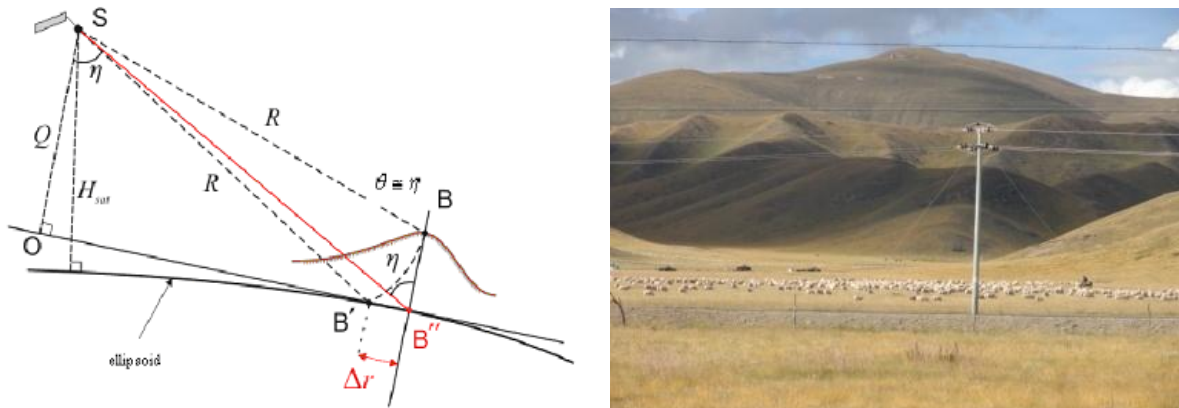

Figure 4-2 Distnace distortion correction geometry adapted from ASAR Product Handbook (2002) (left) and land scape of the study area (right)

Figure 4-2 shows distance distortion geometry correction that was applied to all ASAR WSM images and the rolling terrain picture of the study area.

The incidence angle of ASAR WSM ranges from 15 degree to 45 degree. The ASAR observations acquired at range of incidence angle (15⁰ to 45⁰ have been normalized to an incidence angle of 23 degrees using equation 4-3 below:

$$\sigma^0_{(23)} = \frac{cos^2(23)}{cos^2(\theta_i)} * \sigma^0_{(\theta_i)}$$ Equation 4-3

Where $\sigma^0_{(\theta_i)}$ is the angle dependent backscattering measurement; $\sigma^0_{(23)}$ is the backscattering normalized to an incidence angle of 23, (θ_i) is the actual incidence angle in degrees.

This approach is based on Lambert's law for optics, which assumes that the relationship between the incidence angle and amount of scattering per unit surface area follows the cosine law. This behaviour is typically observed over the middle range of incidence angles, in which ASAR WSM observations have been acquired (Van der Velde et al., 2008).

The average ASAR WSM backscattering coefficient from homogeneous areas (3 × 3 pixel square window, 450 m × 450 m in size) surrounding each soil moisture stations were extracted. The coordinate (latitude and longitude) of the twenty soil moisture station were used as a centre coordinate of the area.

Darker region in ASAR WSM image represent lower backscattering where only very little of radiant energy was reflected back to radar and brighter region represent high backscattering where high portion of radiant energy was reflected back. Wetter target appears brighter and drier surface appears darker with the exception of water surface which act as smooth surface and reflect the incident radiation away from the sensor unless the water wave made the surface rougher.

Yellow river appears darker on ASAR WSM images during summer season which indicates low backscattering response due to specular reflection. The temperature drops below zero degrees Celsius during winter time (especially on January, February), the top river layer freezes. Figure 4-3 shows the seasonal variation of ASAR WSM backscattering. In winter season Yellow river appears brighter and it appears darker during summer season .
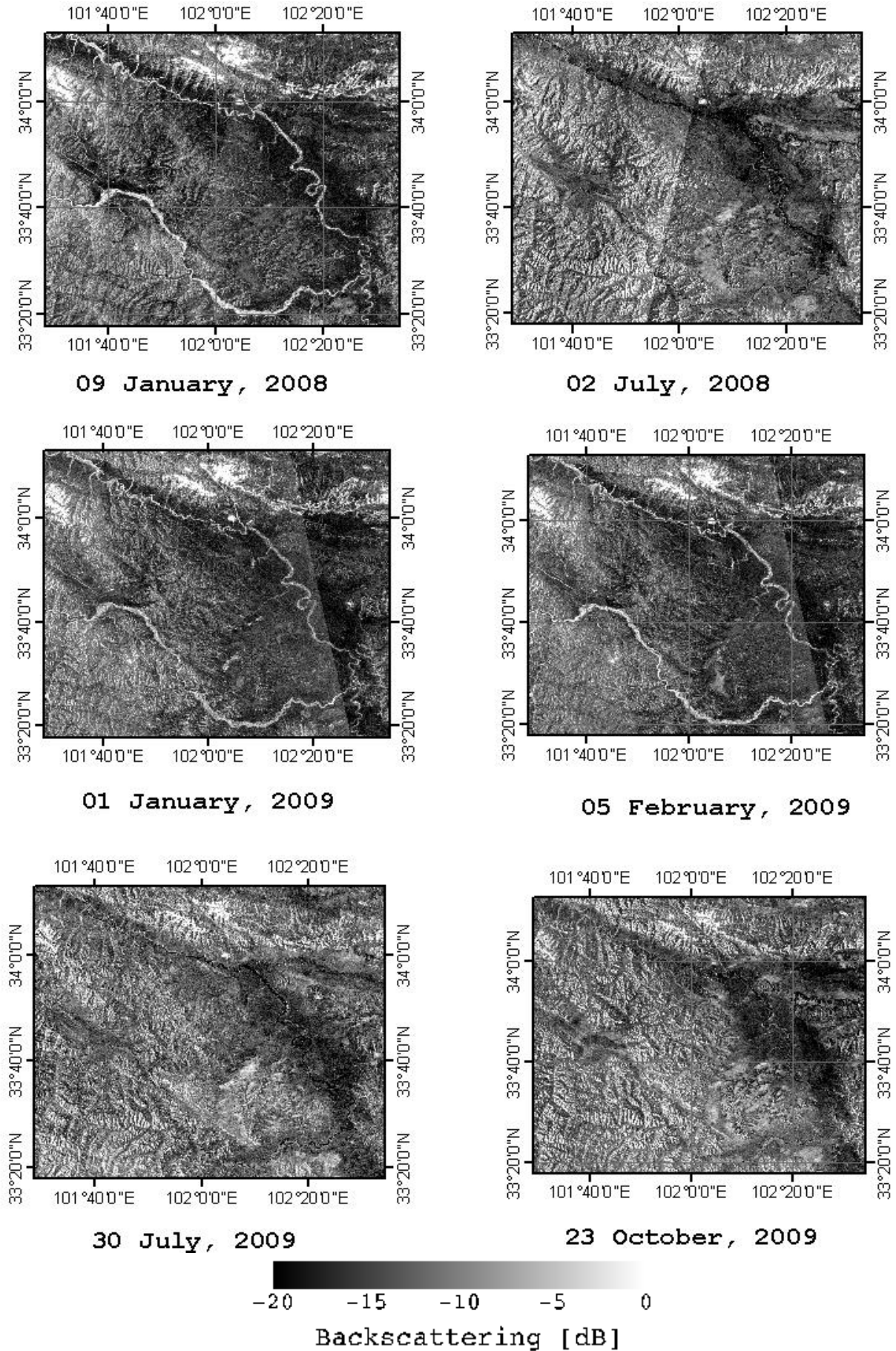
Figure 4-3 ASAR WSM images showing seasonal backscattering variation

4.3.   SPOT NDVI data set

The NDVI data were obtained from 2008-2009, using SPOT VEGETATION product at 1 km spatial resolution. The syntheses of ten consecutive days were obtained as from the 1st to 10th, 11th to the 20th and 21th to end of each month. NDVI product from SPOT 1 km spatial resolution is used to evaluate the vegetation cover. (Image processing and archiving centre, 1998)
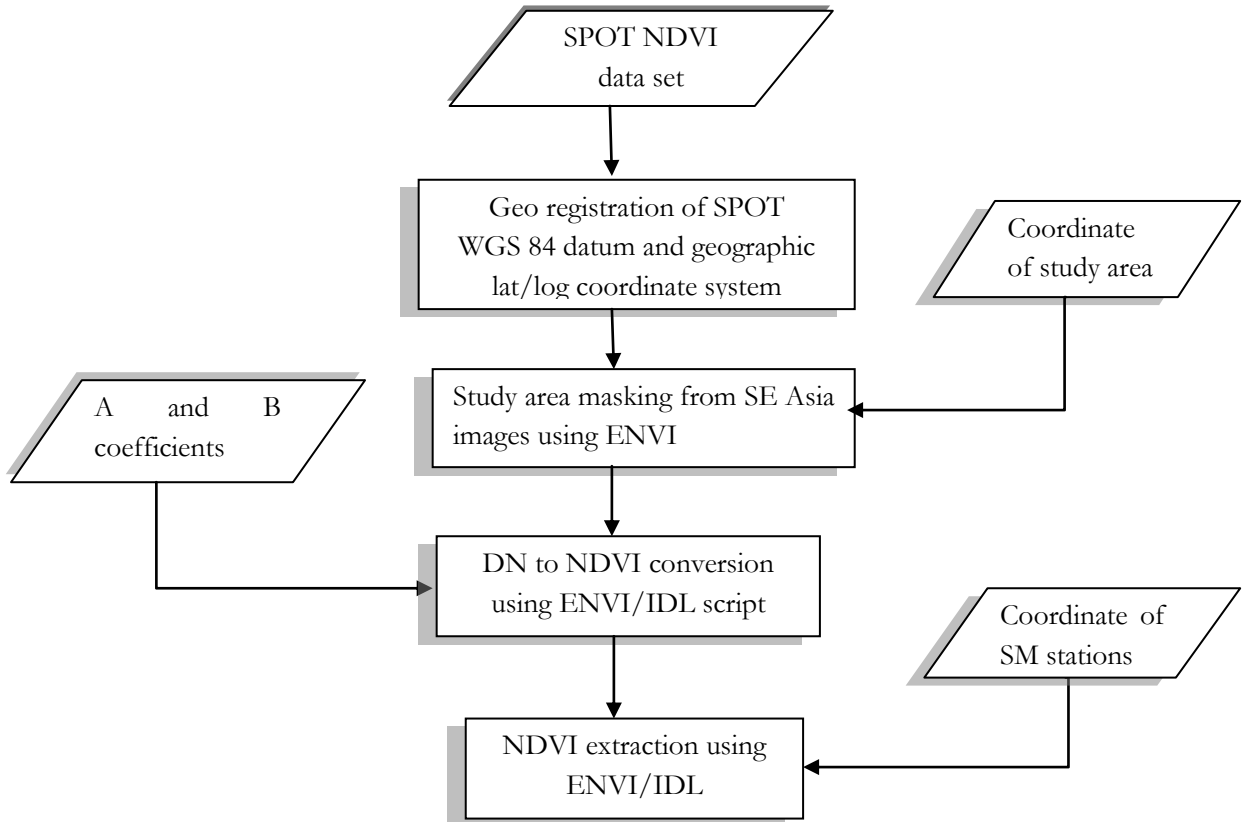
Figure 4-4 Schematization of processing of ASAR WSM images

4.4.   SPOT NDVI derivation and temporal varation anlysis

The NDVI product from SPOT has been processed with ENVI/IDL programming. The images were converted to geographic lat/log with WGS 84 vertical datum. The geographic registration used to extract the study area from the image covering south East Asia.

NDVI value is calculated by equation 4-4 below of each pixel using IDL code.

$$NDVI = a * DN + b \hspace{5cm} \text{Equation 4-4}$$

Where, a is a coefficient = 0.444 and b = -0.1 and DN is Digital number

The average backscattering coefficient and NDVI of all grassland stations were calculated. The coefficient of determination (R^2) and root mean square difference (RMSD) between the mean and each grassland

station were calculated. The result of the analysis is presented in Figure 4-5. The grassland stations are covered by short and homogeneous grass that ranges from approximately 3 cm to 7 cm.
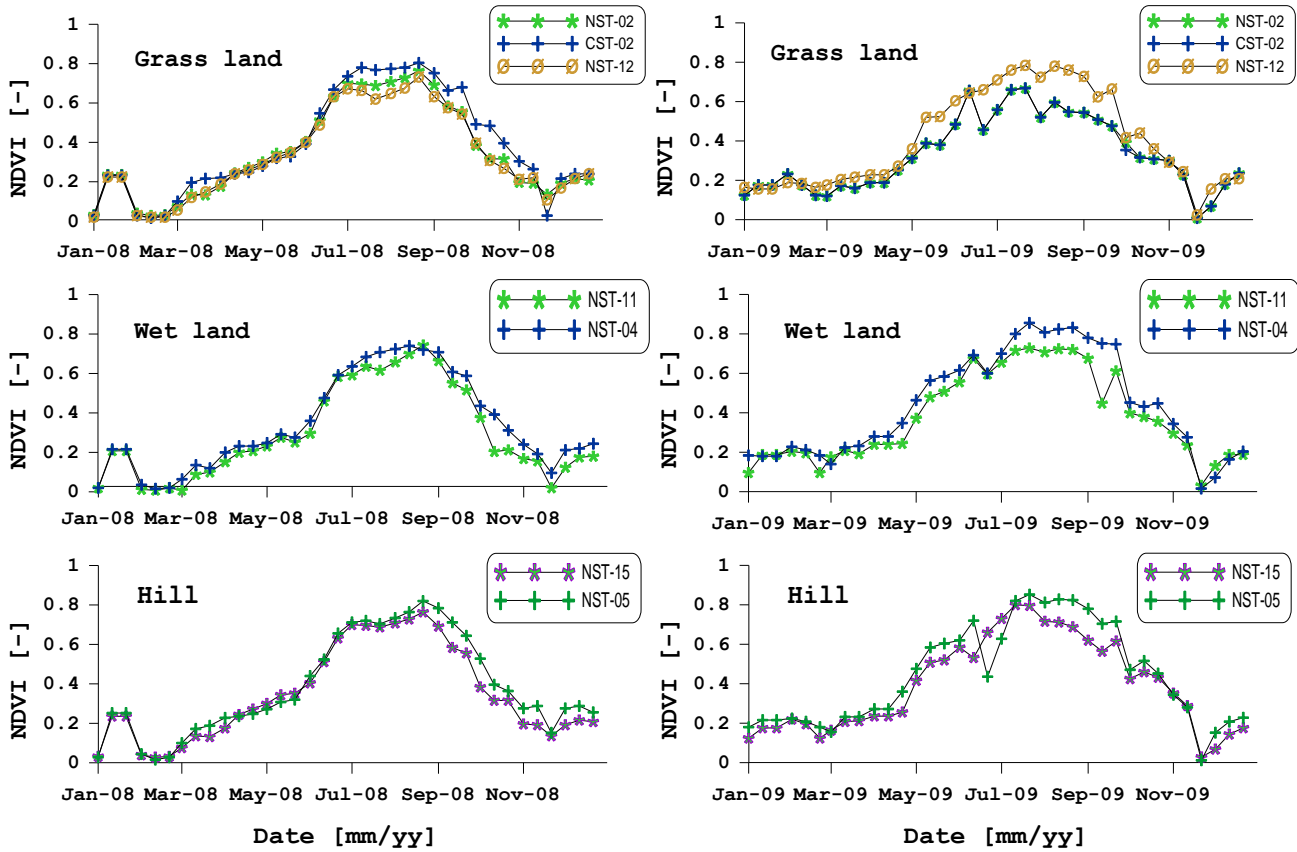
Figure 4-5 SPOT NDVI times series in 2008 and 2009 over grassland, wetland and hill

HDF Viewer was used to read the number of sample (Column) and number of line (row) of the image from the Meta data of the image. Using IDL script the study area between 101-103 East and 33-34 North was masked from image covering SE Asia. One pixel resolution of SPOT NDVI product is 0.0089285714 degree. The size of the catchment is calculated as the difference of maximum and minimum latitude or longitude of the area divided by the SPOT NDVI product pixel resolution.

Time series of NDVI value for the full growth cycle of 2008 and 2009 was extracted over grassland, wetland and hill slope geographical sites. The average NDVI from homogeneous areas (3 × 3 pixel square window, 3 km × 3km in size) surrounding each soil moisture stations were extracted.

5. RESULTS AND DISCUSSION

Maqu catchment is dominantly covered by grassland; however the area also consists of wetlands, hills, river valleys and rolling terrain. In this study, the spatial and temporal variation of ASAR WSM backscattering was analysed in relation to land surface conditions such as vegetation cover, surface soil moisture and soil temperature. In addition, the study analysed the sensitivity of ASAR WSM backscattering to soil moisture and vegetation variation. The geographical study sites selected for this investigation are grassland, wetland and hill slope.

There are 16 grassland stations in Maqu catchment. The land cove in this station is homogeneous grass land and with silt loam soil type. The average organic matter content of grassland station is close to 24 g/kg. The mean and the standard deviation of ASAR backscattering and NDVI were calculated to represent the grassland.

In this study, station NST-04 and NST-11 are considered for analysis of wetland area. The two soil moisture stations, NST-04 and NST-11, are installed in wetland area along with yellow river valley. The soil type in both wetland stations is silt loam covered by short grassland range from approximately 3 cm - 10 cm. The wetland stations has high amount of organic matter content of 229.07 g/kg and 135.74 g/kg, respectively. Therefore, the stations water holding capacity would be higher.

NST-05 and NST-15 are soil moisture stations installed on Hill slopes. These stations are selected to represent the rolling terrain topography. The area is covered by short homogenous grass land (3 cm - 10 cm). The soil type in both stations is silt loam. The organic matter content in both hill slope station are close to 22 g/kg. The OMC in hill slope and grassland stations is lower than wetland stations. The result and discussion of this study is presented in four sections below.

5.1. Spatial backscattering variability

In this section, the spatial variability of backscattering over grassland, wetland and hill slope was analysed. The spatial backscattering variability between each grassland station was also evaluated in ascending and descending pass. The backscattering signature of yellow river at three arbitrary transect were also analysed during winter time.

5.1.1. Backscattering over grassland, wetland and hill slope

The soil texture of the Maqu catchment is dominantly silt loam. Sandy-loam soil type also exists in one of grassland stations. Silt loam (fine textured) has larger surface area and has high water holding capacity whereas sandy-loam (coarse textured) has larger particle size and small surface area and has lower water holding capacity.

The water holding capacity of a soil will increase with increasing of organic matter content. The wetland stations (NST-04 and NST-11) have the higher organic matter content (135 and 229 g/Kg) and this indicates both stations have high water holding capacity. The higher water content in wetland area results high backscattering response as shown in Figure 5-1.

The ASAR WSM backscattering over grassland wetland and hill slope shows similar trend. The lowest backscattering value during winter is approximately 16 dB and highest record during summer is

approximately 8 dB. Compared to the grassland and hill slope stations, wetland stations show the lowest backscattering signature during winter time. The backscattering signature ranges between 5 dB to 15 dB in most cases with the exception of hill slope observation during summer time (especially August) which shows high backscattering response.
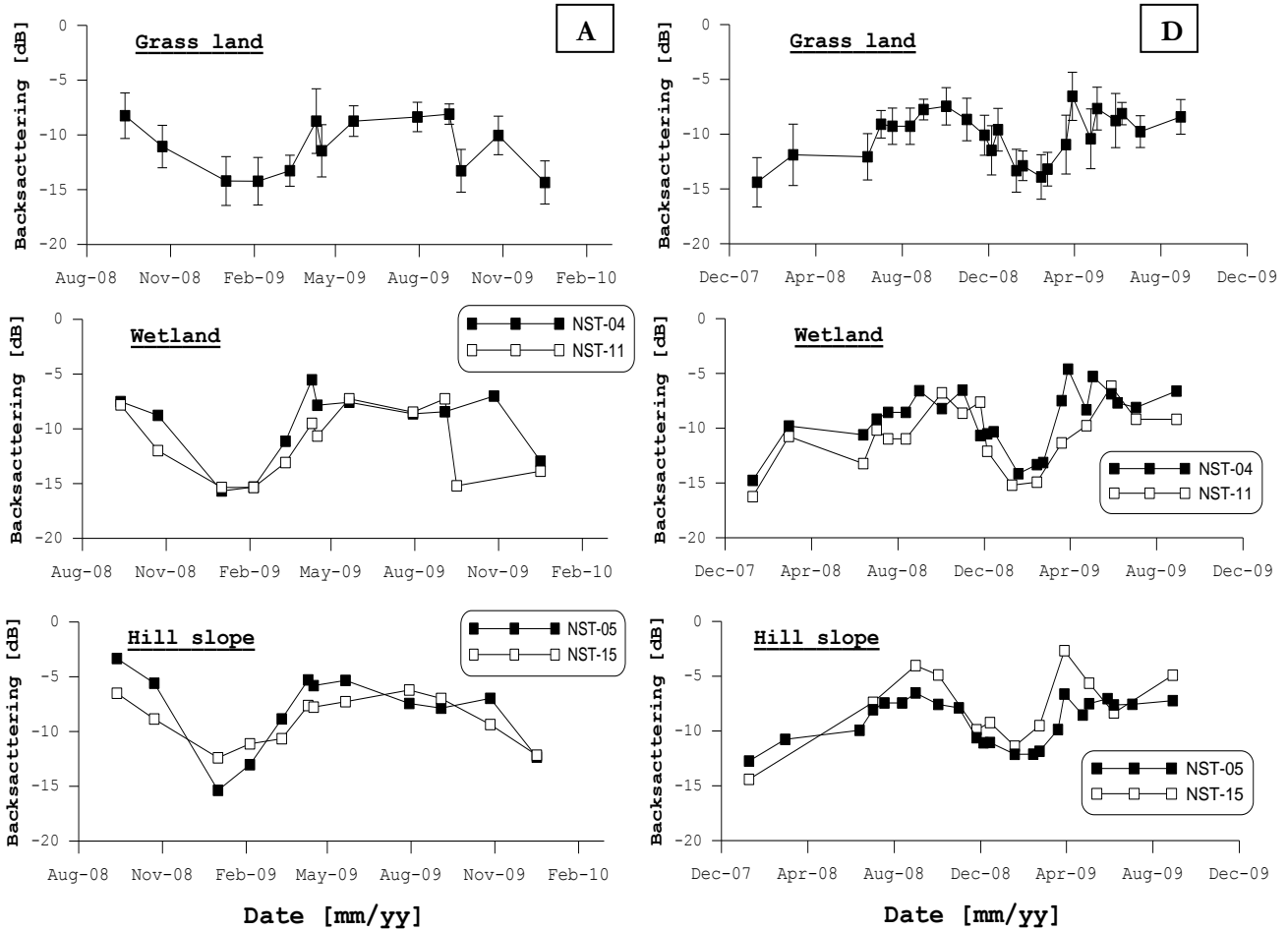

Figure 5-1 Time series ascending (A) and descending pass (D) backscattering trend

Figure 5-1 shows, the time series ARAR WSM backscattering coefficient in ascending and descending pass. The backscattering trend shows decreasing trend during winter time and increasing trend during summer time. The plots show an upward parabolic shape for all cases (grassland, wetland and hill) in ascending and descending pass. The graph has a vertex of low backscattering in winter season, especially in February. The soil temperature, as shown in figure 3.3-3.5, drops below zero during winter time.

The average spatial backscattering variability from mean among grassland station was ± 2 dB. The grass land stations have a backscattering coefficient of -14 dB on 13 February, 2009. The wetland stations (NST-04 and NST-11) shows low backscattering -15 dB. From May to September, when the area receives rainfall, the backscattering increases to -6. In the ascending orbit graph of wetland and grassland, there is an outlier backscattering measurement in HH polarization taken on pass16-Sep-09. The low backscattering response during winter time could be the result of frozen soil. Schwank et al., (2004) expressed the similarity between very dry soil and frozen soil. Therefore the result is as expected. The backscattering during winter time is low (~-15 dB) and high during monsoon season (~-5 dB).

5.1.2.   Backscattering profile of Yellow river

Yellow rivers play an important role in the water resource distribution, particularly in winter, when the land surface runoff is minimal. However, the presence of an ice cover will affect stream flow, modify the ecosystem, restrict navigation and influence hydropower generation (Bernier et al., 2005). The spatial backscattering variability on yellow river has been analysed during winter time.

Three transects across yellow river were taken at three arbitrary locations on ASAR WSM image acquired on 09 January 2008 in VV polarization.
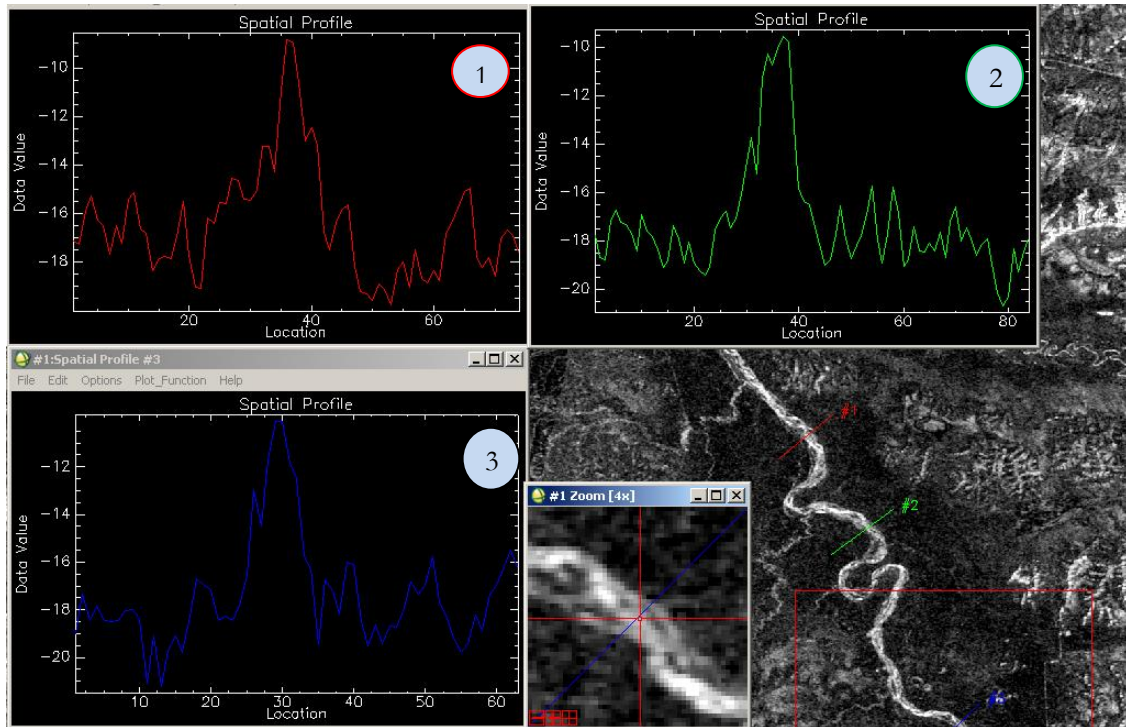

Figure 5-2 Spatial profile of Yellow river at three arbitrary transect during winter season

Figure 5-2 shows the spatial profile of ASAR WSM backscattering coefficient (EVISAT ASAR Product Handbook) at three locations across yellow river. The peak backscattering signature lies on the middle of the river in all three cases and drops on the side banks. The profile shows low backscattering signature along the river and high backscattering on the river.

The low backscattering signature form the side bank of the river could because of the frozen soil layer. The low backscattering response also shown over the time series of ASAR WSM backscattering observation in ascending and descending pass in grassland, wetland and hill slope stations (Figure 5-1). This suggests the soil was frozen on 09 January 2008 and it could be the reason for the low backscattering response from the side bank (Bernier et al., 2005; Rignot & Way, 1994; Wegmüller, 1990).

The high backscattering response over yellow river could be because of volume scattering from frozen top water layer (Langley et al., 2007). The reason is that, the incidence radar signal penetrates the frozen ice pack lying on the river and results volume scattering inside the ice pack and the returned signal became higher and appears brighter on ASAR WSM images. However, the roughness at the ice-water interface could also be the dominant factor for high backscattering response(Bernier et al., 2005).

5.1.3. Spatial backscattering variability among grassland stations

Coefficient of determination (R^2), Root Mean Square Difference (RMSD) and Bias of the sixteen grassland station were calculated. Figure 5-3 shows high coefficient of determination and small RMSD and bias among grassland stations with the mean. However, low coefficient of determination (0.6) and high RMSD (3 dB) and bias (+3 dB) is observed on station NST-06 in both ascending and descending observation. Next to station NST-06 the second lowest coefficient of determination is observed in station NST-09 (0.7).
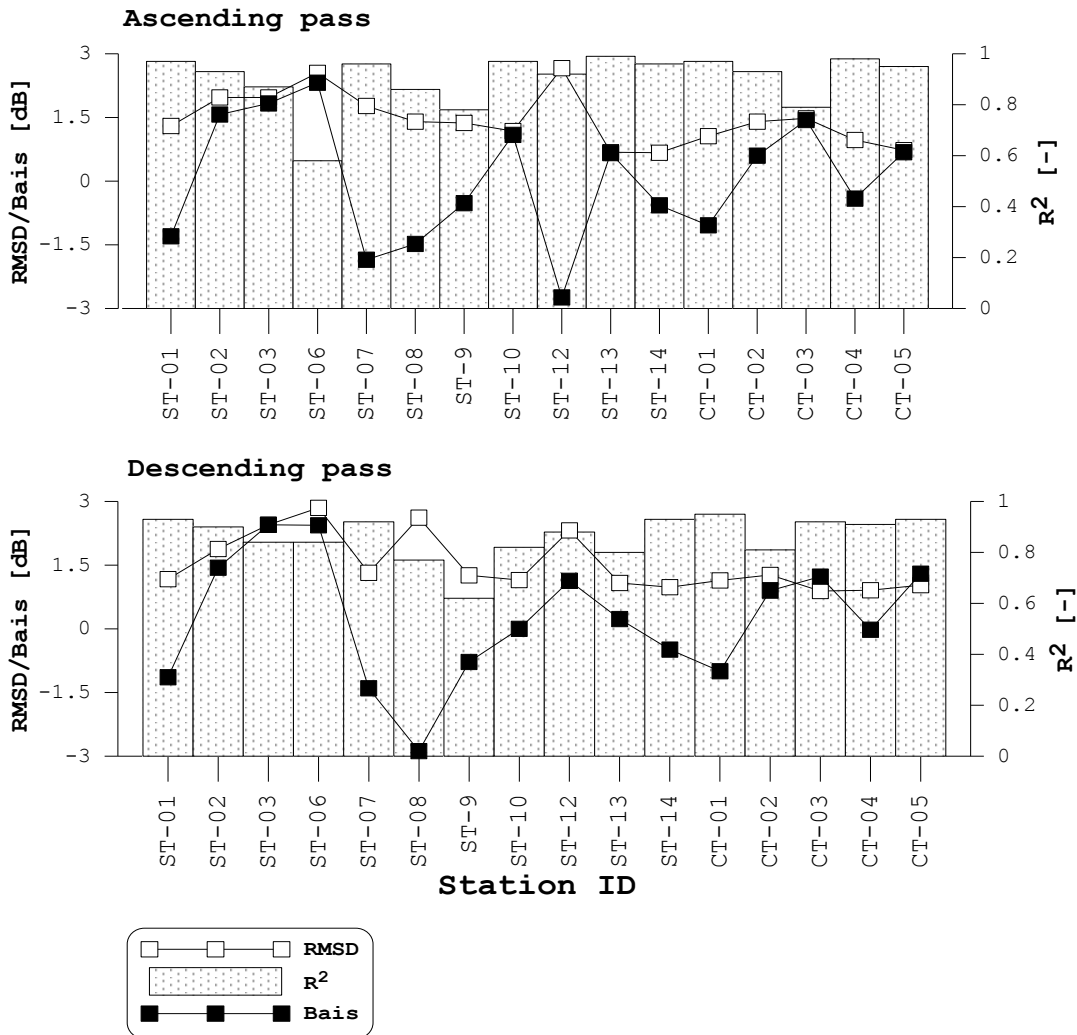
Figure 5-3 Backscattering variation among grassland stations with mean backscattering

The variation in backscattering signature in station NST-06 and NST-09 was higher as shown in figure 5-3 compared to other grassland stations. Station NST-06 was installed in degraded grassland and NST-09 was installed in sandy-loam soil texture. The soil texture and vegetation cover makes these stations different from the rest. This implies the backscattering response from sandy-loam soil texture and degraded grassland cover could be different because of difference in vegetation attenuation, vegetation water content and evaporation rate.

The backscattering coefficient is a function of the soil dielectric constant, the surface roughness and the radar configuration (frequency, polarization and incidence angle). For the same radar configuration the soil texture and vegetation cover of the two grassland stations has shown impact on backscattering signal.

5.2. Temporal backscattering variability

Sensitivity of radar backscattering to the dielectric property suggests significant changes in backscattering are expected with season due to freezing temperature, snow, vegetation change and rainfall. To evaluate the temporal backscattering variability, ASAR WSM (VV and HH polarization) ascending and descending pass observations are plotted in Figure 5-4 and Figure 5-5 over grassland, wetland and hill slop.
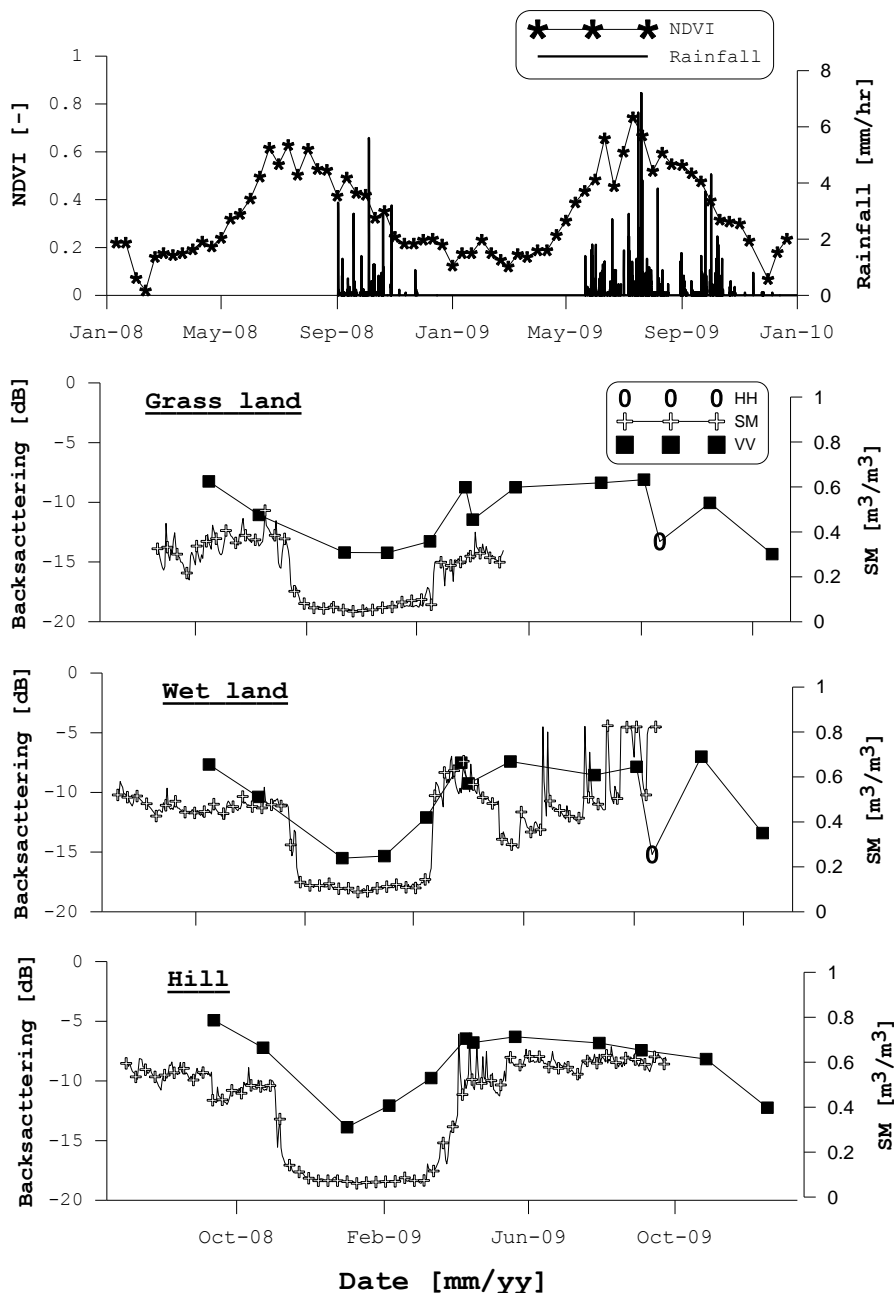
Figure 5-4 VV and HH polarized backscattering ascending trend

Figure 5-4 shows low backscattering signature from December through March and high backscattering signature from May through September. The backscattering coefficient trend shows clear distinction between winter season and summer season. The winter season in the study starts from December to March. January and February are the coldest month of the year. The area gets considerable rainfall from Asian monsoon in summer time starting from May through September. The area receives high amount of rainfall on July and August.

During winter time the soil temperature is below zero degrees celcius and this indicates the soil during winter was frozen soil. Frozen soil contains only little liquid water and this liquid water mainly determines the effective dielectric constant of the soil. The water molecules are in a crystal state scatters low microwave signal (Rignot & Way, 1994). The backscattering coefficient of ASAR WSM (approximately -15 dB) during winter time is as expected. This is in agreement with previous studies that the dielectric property of frozen soil gives lower backscattering response (Wegmüller, 1990).
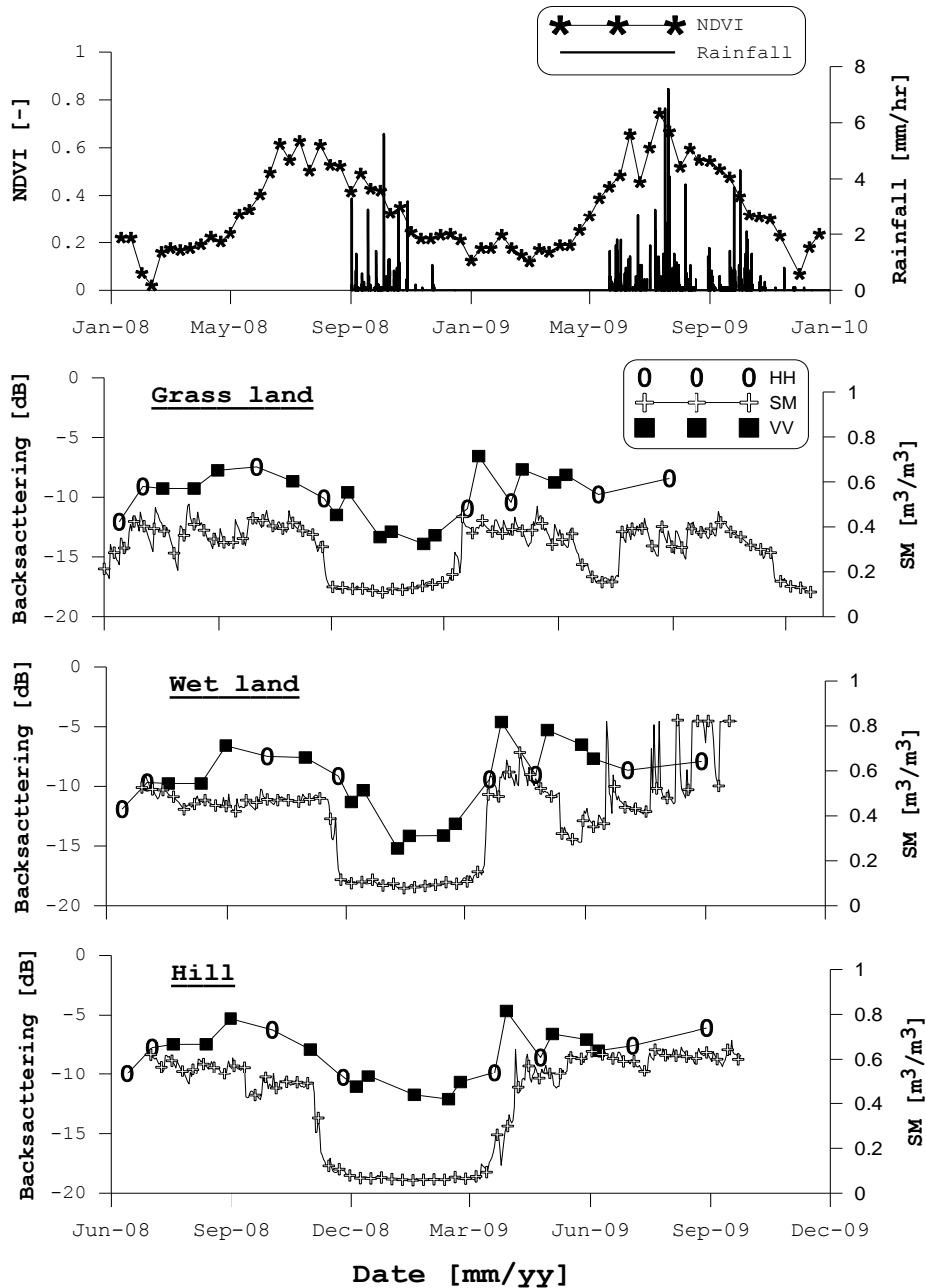
Figure 5-5 Time series VV and HH polarized backscattering descending trend

Towards the summer the area vegetation cover (NDVI) increases gradually and reaches maximum when the rainfall is at the peak intensity. The soil moisture and soil temperature declines during winter time. The backscattering coefficient increases by 10 dB towards the summer season. The shift in backscattering signature follows the monsoon rainfall, the soil moisture state and vegetation covers. The shift in backscattering is more pronounced in wetland areas than grassland and hill slope stations.

Previous studies showed that VV polarization is more sensitive to soil moisture variation than HH polarization (Joseph et al., 2008). However, Figure 5-4 and Figure 5-5 shows similar trend in VV and HH polarization. From the available data set, it is difficult to suggest the change in land surface conditions (Soil moisture and NDVI) have effect on the backscattering signature of VV and HH polarization.

5.3. The effect of soil moisture on backscattering

Advanced Synthetic Aperture Radar (EVISAT ASAR Product Handbook) backscattering signal has shown sensitivity to soil moisture(Loew et al., 2006; Zhang et al., 2009) and previous studies showed that linear relationship exists between soil moisture and backscattering (Moeremans & Dautrebande, 2000; Zribi et al., 2003). In this section, ASAR WSM backscattering coefficient versus in situ soil moisture measurement was linearly fitted in both ascending and descending observation mode. The regression was analysed on grassland, wetland and hill slope stations.
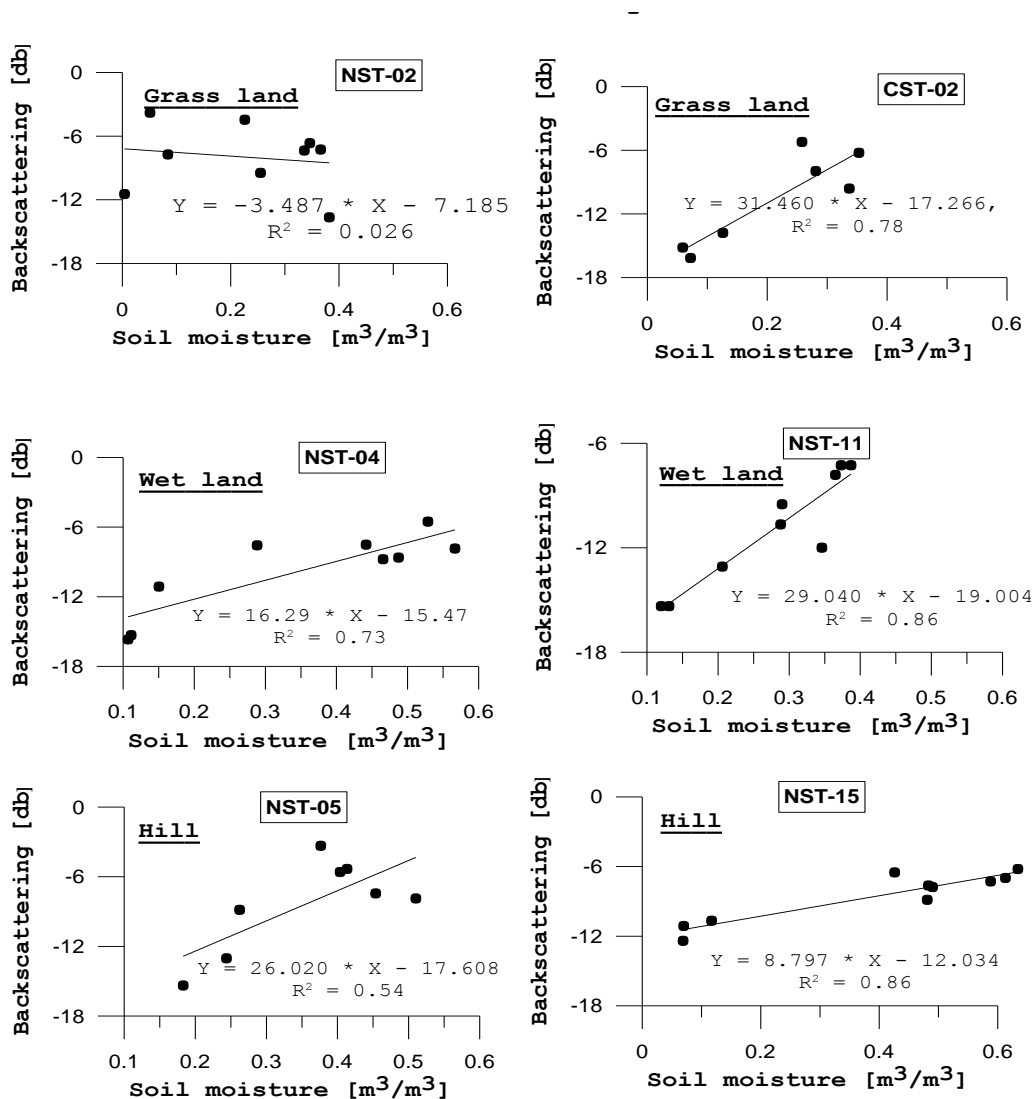

Figure 5-6 Ascending pass correlation between soil moisture and backscattering

Figure 5-6 shows the backscattering coefficient observation of ASAR WSM and the soil moisture at the time of the satellite overpass. It shows high correlation between soil moisture and backscattering coefficient. Mathieu et al. (2003) also found that the average SAR backscatter was well correlated with

seasonal soil moisture variation ($R^2=0.75$). The sensitivity of backscattering to soil moisture is in general decreased by the presence of a vegetation cover. This is due to increased scattering and attenuation of the electromagnetic signal (Wagner et al., 1999). However, the coefficient of determination in grassland, wetland and hill slope was high (R^2 from 0.73 up to 0.86).
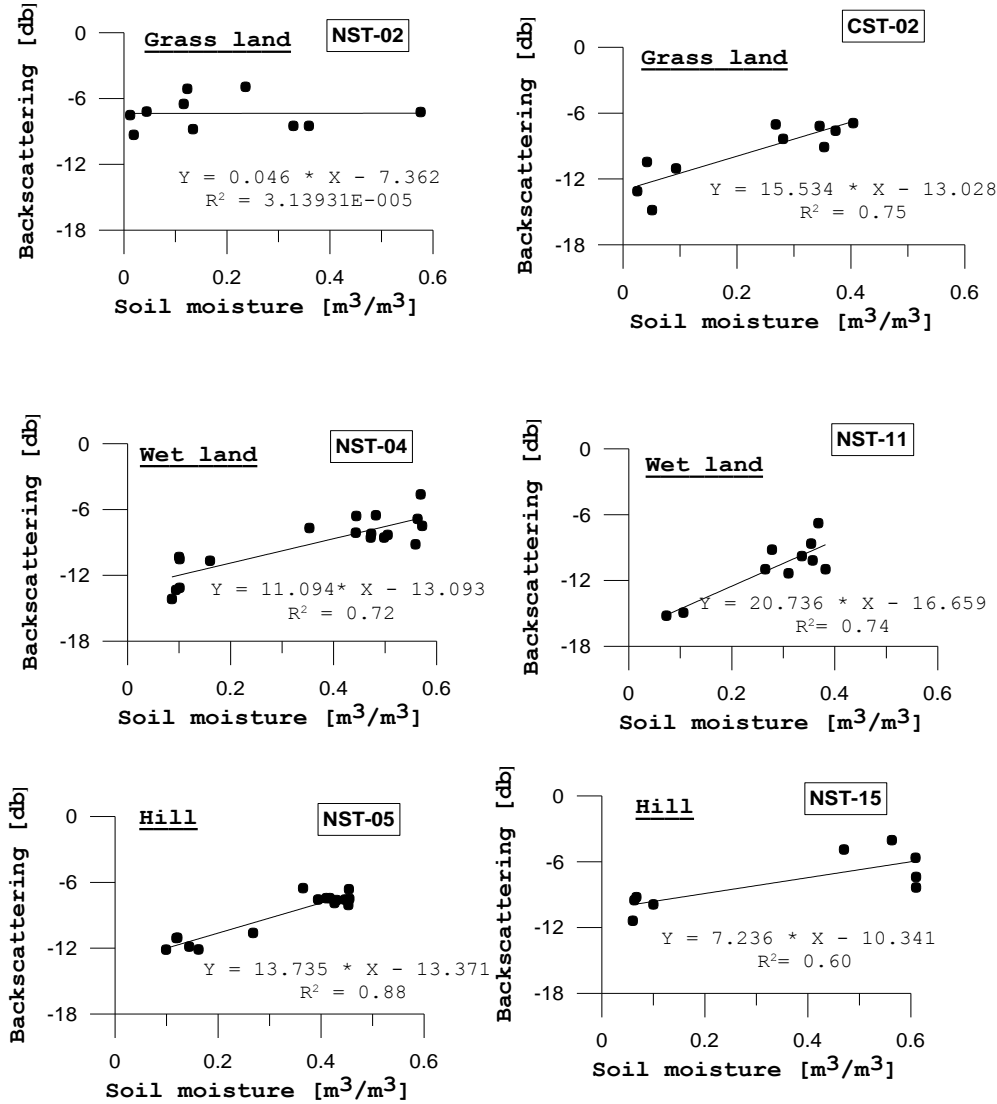
Figure 5-7 Dscending pass correlation between soil moisture and backscattering

Figure 5-6 and Figure 5-7 clearly shows high correlation between backscattering coefficient and soil moisture over grassland, wetland and hill stations. The high correlation between soil moisture and ASAR backscattering implicitly indicates the backscattering is dependent on the soil moisture. This is in agreement with Zribi et al., (2003) that showed the volumetric soil moisture content up to 35-40% by volume is linearly related to the backscattering coefficient. This linear relationship could also be applied to the ASAR WSM images to map soil moisture over the study area.

$$M_v = A + B * \sigma^0 \hspace{5cm} \text{Equation 5-1}$$

Where A and B are constants to be obtained from soil moisture and backscattering coefficient graph and are not exactly the same from one catchment to the other, σ^0 is ASAR WSM backscattering coefficient and M_v is soil moisture content (EVISAT ASAR Product Handbook).

The ascending pass coefficient of determination (R^2) of the hill slope stations, NST-05 and NST-15 is 0.54 and 0.86, respectively. However, the descending pass coefficient of determination (R^2) is 0.88 and 0.6. The result shows NST-15 has high correlation in the ascending pass and NST-05 has high correlation on descending pass, on the other hand NST-15 has lower correlation in the ascending pass and NST-05 has lower correlation on descending pass. The higher and lower correlation of backscattering with soil moisture on ascending and descending pass on the hill slope stations (NST-05 and NST-15) could be the orientation of the station with respect to the satellite pass. If the hills slope faces the satellite pass (either in ascending or descending pass), the returned backscatter signal towards the satellite could be higher and vice versa.

Table 5-1 Trend line coefficients of ascending and descending pass correlation with Soil moisture

Study sites	Station ID	Coefficient	Ascending	Descending
Grassland	NST-02	A	-3.49	0.05
		B	-7.19	-7.33
		R^2	**0.03**	**0.00**
	CST-02	A	31.46	15.34
		B	-17.27	-13.02
		R^2	**0.80**	**0.75**
Wetland	NST-04	A	10.62	11.04
		B	-13.86	-13.09
		R^2	**0.53**	**0.72**
	NST-11	A	29.04	20.74
		B	-19.01	-16.66
		R^2	**0.86**	**0.74**
Hill slope	NST-05	A	26.02	13.735
		B	-17.61	-13.371
		R^2	**0.54**	**0.88**
	NST-15	A	8.80	7.24
		B	-12.03	-10.34
		R^2	**0.86**	**0.60**

However, the high correlation result between soil moisture and ASAR WSM backscattering was in contradiction with Kasischke et al., (2009) that found no correlation in Alaskan wetland complex. "Across all sites, we found no correlations between ERS SAR backscatter and soil moisture. This lack of correlation was most likely due to the fact that there was variable vegetation cover and structure between the different sites that also contributed to variations in radar backscatter." (Kasischke et al., 2009).

The major difference between this two study areas (Maqu Catchment and Alaska Wetland) is the vegetation cover. The vegetation cover in Maqu Catchment was homogeneous grassland that could have

constant contribution for ASAR WSM backscattering. The effect of vegetation on ASAR WSM backscattering will be discussed on section 5.4.

5.4.   The effect of vegetation on backscattering

The vegetation layer in Maqu study area is primarily short homogeneous grass. The vegetation absorbs and scatters some of the microwave radiation signal. The absorption is primarily due to the water content in the vegetation and the scattering is primarily due to the geometry of the grass canopy. (Yisok et al., 2007) Because of its complex geometry the precise amounts of absorption and scattering are difficult to estimate.

The total returned backscattering signal towards the sensor is a contribution from the soil surface (soil moisture content and roughness) and the vegetation geometry regardless of the sensor configuration (frequency, wave length and view angle). Therefore, ten days syntheses of SPOT NDVI were used to investigate the temporal variability vegetation cover from 2008 through 2009. The correlation between NDVI and ASAR WSM backscattering coefficient were computed over grassland, wetland and hill slope.
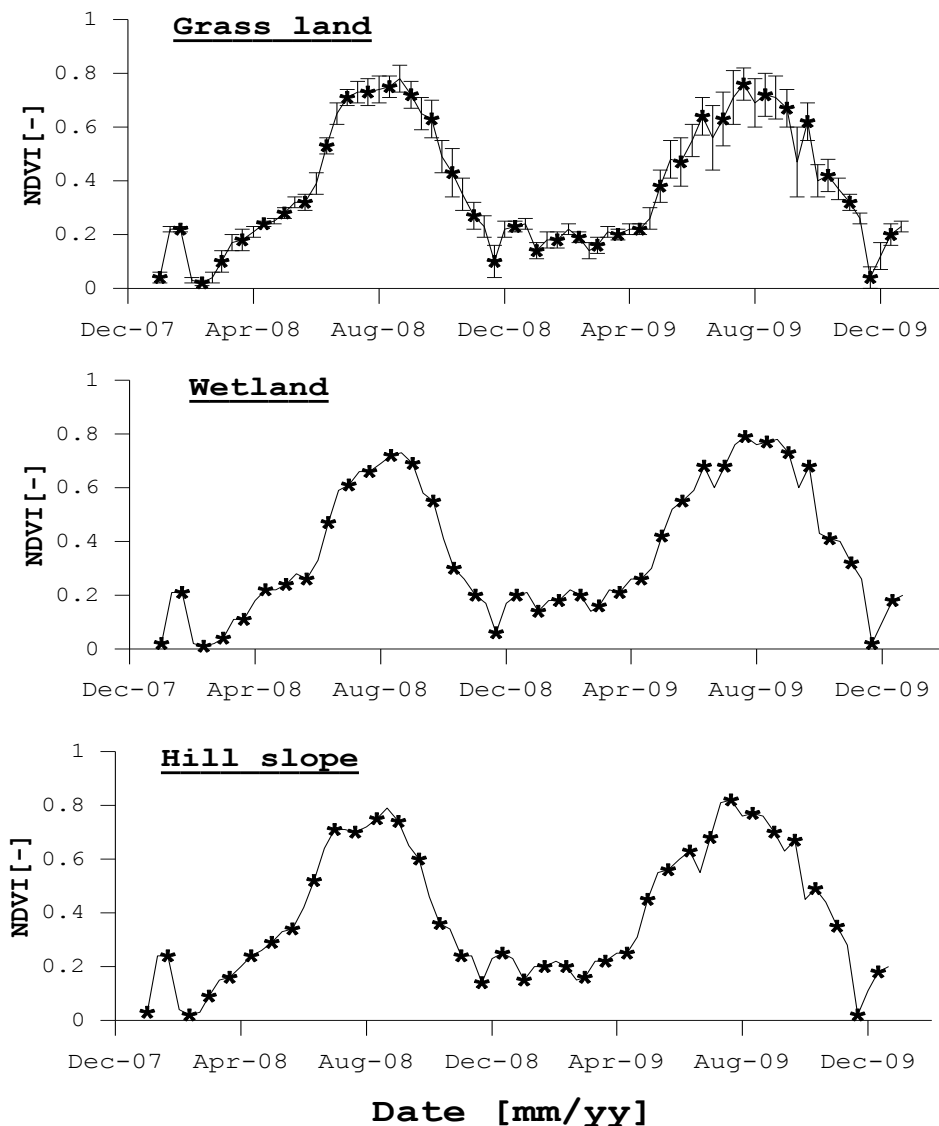

Figure 5-8 SPOT NDVI time series over grassland, wetland and hill

Figure 5-8 shows clear distinction between monsoon season and winter season. The standard deviations of the sixteen grassland stations were plotted as error bar in Figure 5-8. The grassland station has smaller deviation from the mean throughout the year (less than 0.05). The mean NDVI value has been taken for wetland (NST-04 and NST-11) and hill slope station (NST-05 and NST-15). The NDVI value increases starting from May and reaches to maximum on August in all stations. The maximum NDVI value in grassland, wetland and hill slope is approximately 0.8 during monsoon season (Jun, July, August) and the minimum value is close to 0.2 during winter season (December, January and February). The area gets considerable amount of rainfall in monsoon season (refer Figure 3-3).

The NDVI trend over grassland, wetland and hill has the same pattern during the year 2008 and 2009. Similar NDVI trend between grassland, wetland and hill slope indicates the homogeneity of the area. The increasing NDVI trend suggests that the response to rainfall input is high, particularity the monsoon period.

In both years, the peak NDVI was recorded during August when the area receives high amount of rainfall. The lower NDVI record was during February when the area was cold and dry. The vegetation biomass varies in accordance with rainfall pattern. The seasonal change of vegetation cover was as expected.

To check the mean NDVI value of the grassland stations was representative or not, the root mean square difference (RMSD) and the correlation were calculated. The result of the analysis is presented in Figure 5-9 below.
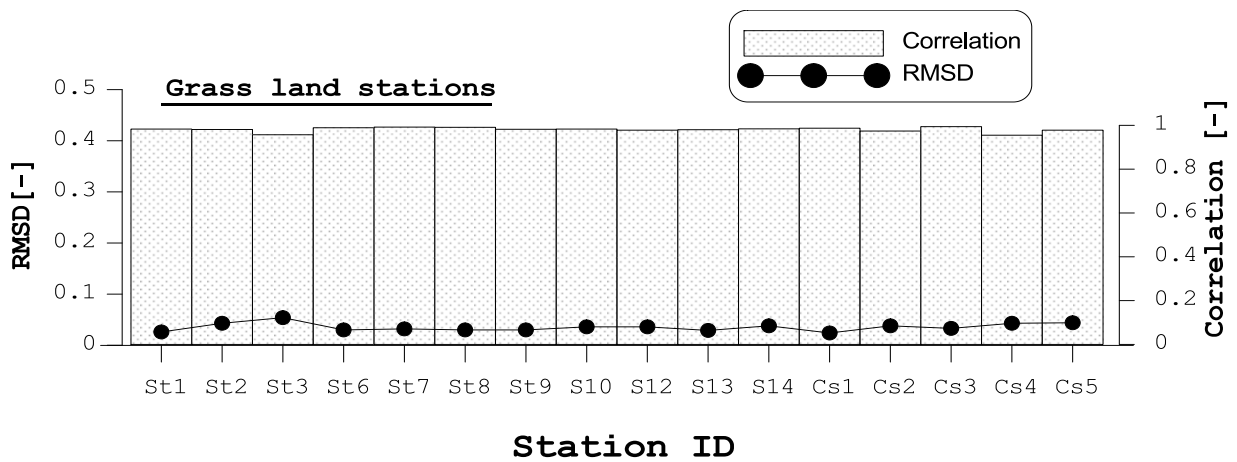
Figure 5-9 Correlation and RMSD between all grassland station

Figure 5-9 shows high correlation between grassland stations and the mean NDVI. The presented result shows very high coefficient of determination between the mean NDVI and all grassland station ($R^2 > 0.9$) and very low Root Mean Square Difference (RMSD<0.05).

The result verifies the homogeneous grass cover of the Maqu region and the change in the vegetation cover over all the grassland station throughout the year is similar. Therefore, the mean NDVI of all grassland station can be considered for comparison with wetland and hill slope station NDVI values.

The effect of vegetation on ASAR WSM backscattering VV (vertical) and HH (Horizontal) polarization was analyzed fitting the NDVI and backscattering linearly. The correlation between NDVI and HH/VV polarized backscattering coefficient is presented below in Figure 5-10 and Figure 5-11.

NDVI and HH polirized backscattering

Figure 5-10 Correlation between NDVI and HH polarized backscattering coefficient

Figure 5-10 shows linear regression fit between HH polarized ASAR WSM backscattering versus NDVI. The figure shows low coefficient of determination (R^2) between grassland stations and the mean NDVI.

The coefficient of determination between HH polarized ASAR WSM backscattering coefficient and NDVI was less than 0.3 except station NST-05 which has 0.77. The variation of ASAR WSM backscattering for change in NDVI value is small.

This suggests even the change in vegetation cover is large (NDVI from 0.2 up to 0.8); the sensitivity of backscattering to change NDVI is mall. The reason could be the homogenous grass cover of the area contribute constant toward the ASAR backscattering signal.
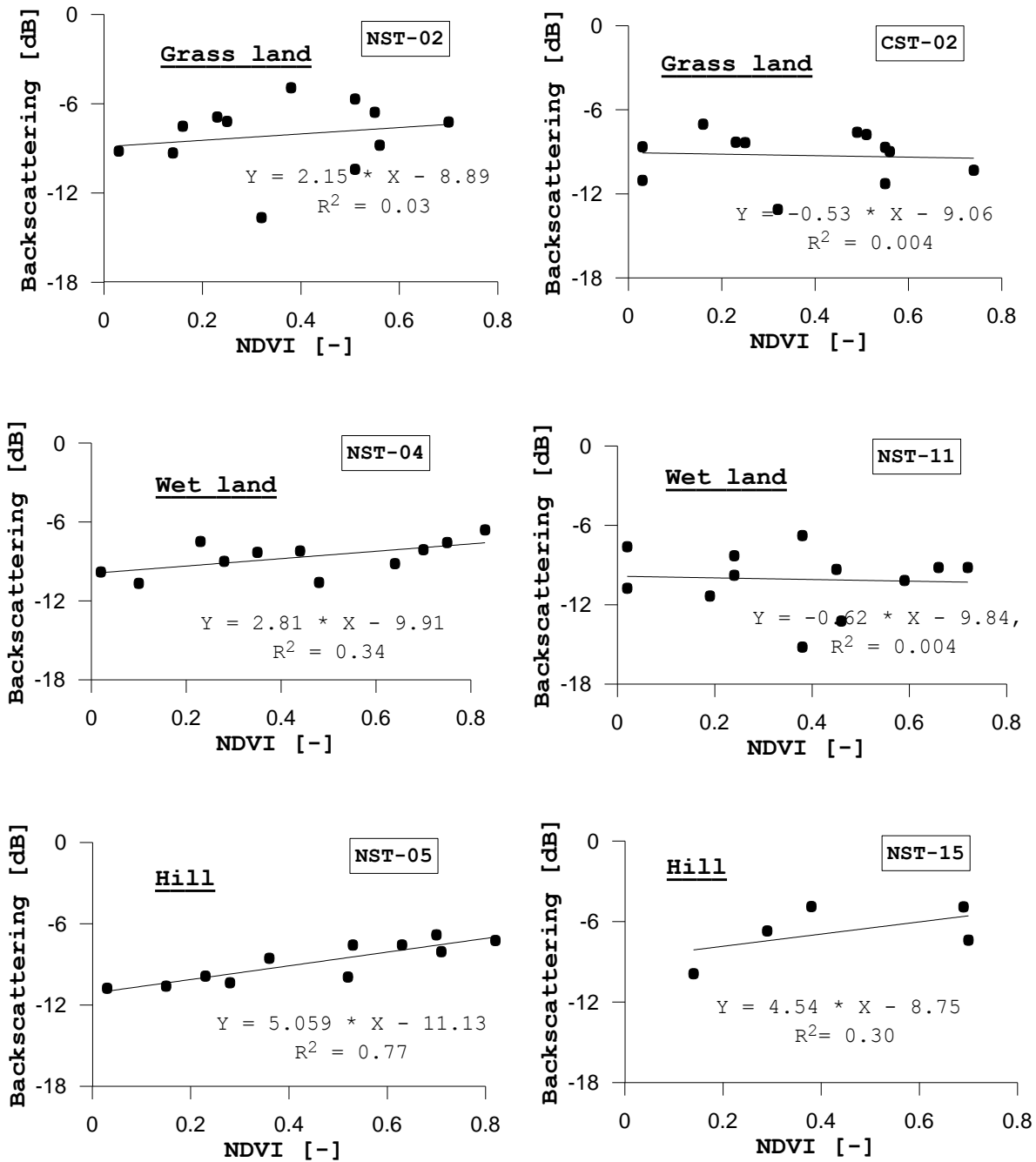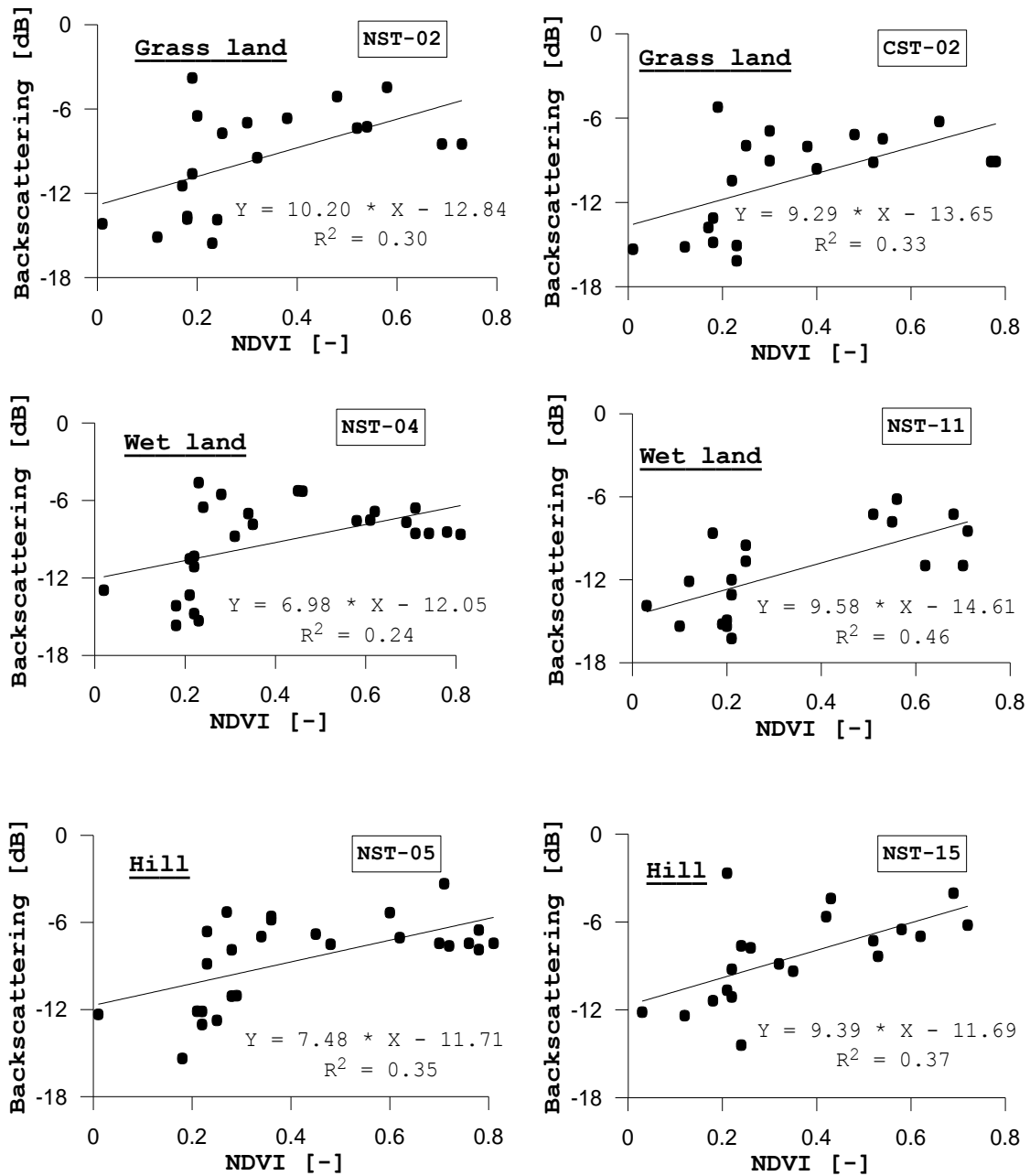
NDVI and VV polirized backscattering

Figure 5-11 Correlation between NDVI and VV polarized backscattering coefficient

Figure 5-11 shows linear regression fit between VV polarized ASAR WSM backscattering versus NDVI. There is low correlation between NDVI and backscattering in both VV and HH polarization in the three

study sites. The slope of the regression line in VV polarized linear fit case is higher than HH polarized fit. This suggests the change in NDVI is more pronounced in VV polarization than HH polarization. However, it is difficult to conclude that VV polarized ASAR WSM data is more sensitive to vegetation cover change, because the coefficient of determination shows low value (less than 0.46).

The ASAR WSM backscattering observation has been normalized to 23 degree incidence angle. Previous studies found out that scattering from soil surfaces is very important at angles near nadir, while the vegetation volume scattering is dominant at larger incident angles (> 30°) (Tsan et al., 1984). A radar pulse reflected from a vegetation-covered soft surface is subject to two way attenuation and scattering by the vegetation layer.

Table 5-2 Correlation coefficients of NDVI and HH polarized backscattering coefficient

Study sites	Station ID	Coefficient	VV pol	HH pol
Grassland	NST-02	A	10.20	2.15
		B	-12.84	-8.89
		R²	**0.30**	**0.03**
	CST-02	A	9.29	-0.53
		B	-13.65	-9.06
		R²	**0.33**	**0.004**
Wetland	NST-04	A	6.98	2.81
		B	-12.05	-9.91
		R²	**0.24**	**0.34**
	NST-11	A	9.58	-0.62
		B	-14.61	-9.84
		R²	**0.46**	**0.004**
Hill slope	NST-05	A	7.48	5.06
		B	-11.71	-11.13
		R²	**0.35**	**0.77**
	NST-15	A	9.39	4.54
		B	-11.69	-8.75
		R²	**0.37**	**0.30**

6.   CONCLUSIONS AND RECOMMENDATIONS

6.1.   Conclusions

The temporal dynamics of ASAR WSM backscattering has been evaluated over the eastern part of the Tibetan Plateau, which is dominated by grassland, wetland and hill slope. The seasonal variation (cold winter and rainy summer) primarily affected the backscattering response in the Maqu catchment.

The ASAR WSM observation over the Maqu region has low backscattering during winter time and high backscattering during summer time. The reason for change in backscattering coefficient could be the change in surface roughness, soil moisture content and vegetation attenuation. Since the area is dominantly used for grazing, the change in roughness through agricultural practice such as ploughing is negligible. The homogenous grass cover evenly contributes to the backscattering over the study area. Therefore, soil moisture which very dynamic spatially affect the backscattering response in this area. This verifies the first hypothesis that on Tibetan plateau the homogeneous grassland vegetation has smaller contribution on ASAR backscattering signal than the soil moisture.

Spatial variation of backscattering among grassland station were minimum except two stations (NST-06 and NST-09) which has lower correlation, RMSD and bias from the mean backscattering. The land cover over station NST-06 was degraded grassland and the soil texture of station NST-09 was sandy loam. The grassland, wetland and hill slope stations have different physiographical characteristics and also have different backscattering response. The land cover, topography, soil texture, organic matter content, soil moisture and soil moisture has effect on backscattering signature however soil moisture variation has the higher impact for change in backscattering. High correlation between ASR WSM backscattering and soil moisture exists and the backscattering increase form winter season to summer when the area gets rainfall and frozen soil melts.

The temporal backscattering signal during winter and summer season was observed as low and high, respectively. During winter season, the soil temperature measurement from Em50 ECH$_2$O data logger drops below freezing point. This indicates the soil layer at the measurement depth (5 cm) was frozen. It shows that the ASAR WSM backscattering signal from frozen soil is low and frozen can be considered as dry soil.

The effect of soil moisture variation on backscattering response was examined as very high. The backscattering response was sensitive to soil moisture change. The correlation analysis (Figure 5-6 and Figure 5-7) shows high coefficient of determination (R^2 > 0.8) between soil moisture and backscattering. When the soil moisture increase the backscattering also increases. The increase in backscattering dynamic due to increase of soil moisture content was as expected. Dobson et al., (1985) also showed that the increase in volumetric water content increase the dielectric constant of the soil at different frequency and hence increase backscattering signal. The relation between soil moisture and backscattering was expressed by linear line with high coefficient of determination up to 0.88. It verifies the second hypothesis that the relationship between soil moisture and backscattering signal can be approximated by linear relationship.

The correlation, RMSD and bias between the mean NDVI and each grassland station were very small. This indicates that spatial and temporal variation in vegetation cover is small. The study area is covered by fairly homogeneous grassland. The correlation between NDVI and backscattering indicates low coefficient

of determination (R² less than 0.3). This shows the effect of vegetation cover on backscattering is low compared to the soil moisture. This could be because of the height of the grass canopy which is short and the microwave radar can penetrate the grass cover without attenuation or the homogeneous grass cover have constant contribution towards the returning signal.

6.2.   Recommendations

The ASAR WSM observation provides a good data set for spatial and temporal backscattering analysis in relation to land surface sate such as soil moisture, soil temperature and vegetation biomass. This data set (ASAR WSM) also showed high correlation with soil moisture variation over the area. The study area (Maqu catchment) is covered by homogeneous grassland. This suggests the backscattering contribution from vegetation layer could be constant. Therefore, it would be a good choice for estimating distributed soil moisture for hydrological modelling; integrated watershed water management and other applications. The surface height variation can be approximated by root mean square height variation (S) and autocorrelation length (l) assuming either Gaussian or exponential function to account for surface roughness contribution. Integral Equation Model (IEM) Advanced Integral Equation Model (AIEM) could be used to simulate the backscattering and mostly soil moisture could also be retrieved using dielectric mixing model (Dobson et al., 1985; Hallikainen et al., 1985).

ASAR WSM observation has fairly high spatial and temporal resolution. The ASAR WSM backscattering coefficient contains information on the dielectric property of the target. The seasonal climatic variation on Maqu catchment has been clearly identified with ASAR WSM and SPOT NDVI observation. The backscattering coefficient from ASAR WSM observation can provide information that can be used for monitoring land surface sate changes. The seasonal thawing\freezing, vegetation cover change (especially over grazing,) and drought can be monitored using ASAR WSM data set.

LIST OF REFERENCES

Attema, E. P., & Ulaby, F. T. (1978). Vegetation modeled as a water cloud. *Radio Science, 13*, 357-364.

Baup, F., Mougin, E., de Rosnay, P., Timouk, F., & Chênerie, I. (2007). Surface soil moisture estimation over the AMMA Sahelian site in Mali using ENVISAT/ASAR data. *Remote Sensing of Environment, 109*(4), 473-481.

Bernier, M., Gauthier, Y., Mermoz, S., Gherboudj, I., El Battay, A., & Khaldoune, J. (2005, 25-29 July 2005). *Investigating polarimetric SAR data for cryospheric monitoring in a Canadian environment.* Paper presented at the Geoscience and Remote Sensing Symposium, 2005. IGARSS '05. Proceedings. 2005 IEEE International.

Bindlish, R., & Barros, A. P. (2001). Parameterization of vegetation backscatter in radar-based, soil moisture estimation. *Remote Sensing of Environment, 76*(1), 130-137.

Cui, X., Graf, H.-F., Langmann, B., Chen, W., & Huang, R. (2006). Climate impacts of anthropogenic land use changes on the Tibetan Plateau. *Global and Planetary Change, 54*(1-2), 33-56.

Dante, L., Vekerdy, Z., Su, Z., & Jun, W. (2009). Continuous in situ soil moisture measurements at Maqu site. *CEOP – AEGIS Technical Report 1(12).*

Decagon Devices. (2007). *EC-TM ECH2O Operation manual.* Pullman, WA 99163 - USA.

Dobson, M. C., Ulaby, F. T., Hallikainen, M. T., & El-Rayes, M. A. (1985). Microwave Dielectric Behavior of Wet Soil-Part II: Dielectric Mixing Models. *Geoscience and Remote Sensing, IEEE Transactions on, GE-23*(1), 35-46.

European Space Agency. (2010). SAR mission. *Web page* Retrieved August 16, 2010, from http://envisat.esa.int/handbooks/asar/CNTR2-11-5.htm

EVISAT ASAR Product Handbook. (2002). European Space Agency. *Web page, 2010*(Augest 3).

Hallikainen, M. T., Ulaby, F. T., Dobson, M. C., El-Rayes, M. A., & Lil-Kun, W. (1985). Microwave Dielectric Behavior of Wet Soil-Part 1: Empirical Models and Experimental Observations. *Geoscience and Remote Sensing, IEEE Transactions on, GE-23*(1), 25-34.

Image processing and archiving centre. (1998). SPOT NDVI product. Retrieved 8 November, 2010, from http://www.spot-vegetation.com/

Joseph, A. T., van der Velde, R., O'Neill, P. E., Lang, R. H., & Gish, T. (2008). Soil Moisture Retrieval During a Corn Growth Cycle Using L-Band (1.6 GHz) Radar Observations. *Geoscience and Remote Sensing, IEEE Transactions on, 46*(8), 2365-2374.

Kasischke, E. S., Bourgeau-Chavez, L. L., Rober, A. R., Wyatt, K. H., Waddington, J. M., & Turetsky, M. R. (2009). Effects of soil moisture and water depth on ERS SAR backscatter measurements from an Alaskan wetland complex. *Remote Sensing of Environment, 113*(9), 1868-1873.

Langley, K., Hamran, S. E., Hogda, K. A., Storvold, R., Brandt, O., Hagen, J. O., et al. (2007). Use of C-Band Ground Penetrating Radar to Determine Backscatter Sources Within Glaciers. *Geoscience and Remote Sensing, IEEE Transactions on, 45*(5), 1236-1246.

Loew, A., Ludwig, R., & Mauser, W. (2006). Derivation of surface soil moisture from ENVISAT ASAR wide swath and image mode data in agricultural areas. *Geoscience and Remote Sensing, IEEE Transactions on, 44*(4), 889-899.

Low, A., Ludwig, R., & Mauser, W. (2005). Derivation of near surface soil moisture patterns from ENVISAT ASAR data. *IEEE International, 4*(05), 404-407

Mathieu, R., Sbih, M., Viau, A. A., Anctil, F., Parent, L. E., & Boisvert, J. (2003). Relationships between Radarsat SAR data and surface moisture content of agricultural organic soils. *International Journal of Remote Sensing, 24*(24), 5265-5281.

Minchella, A., Del Frate, F., Capogna, F., Anselmi, S., & Manes, F. (2009). Use of multitemporal SAR data for monitoring vegetation recovery of Mediterranean burned areas. *Remote Sensing of Environment, 113*(3), 588-597.

Moeremans, B., & Dautrebande, S. (2000). Soil moisture evaluation by means of multi-temporal ERS SAR PRI images and interferometric coherence. *Journal of Hydrology, 234*(3-4), 162-169.

Paloscia, S., Pampaloni, P., Pettinato, S., & Santi, E. (2008). A Comparison of Algorithms for Retrieving Soil Moisture from ENVISAT/ASAR Images. *Geoscience and Remote Sensing, IEEE Transactions on, 46*(10), 3274-3284.

Rahman, M. M., Moran, M. S., Thoma, D. P., Bryant, R., Holifield Collins, C. D., Jackson, T., et al. (2008). Mapping surface roughness and soil moisture using multi-angle radar imagery without ancillary data. *Remote Sensing of Environment, 112*(2), 391-402.

Rignot, E., & Way, J. B. (1994). Monitoring freeze--thaw cycles along North--South Alaskan transects using ERS-1 SAR. *Remote Sensing of Environment, 49*(2), 131-137.

LIST OF REFERENCES

Schmugge, & Thomas, J. (1983). Remote Sensing of Soil Moisture: Recent Advances. *Geoscience and Remote Sensing, IEEE Transactions on, GE-21*(3), 336-344.

Schwank, M., Stahli, M., Wydler, H., Leuenberger, J., Matzler, C., & Fluhler, H. (2004). Microwave L-band emission of freezing soil. *Geoscience and Remote Sensing, IEEE Transactions on, 42*(6), 1252-1261.

Su, Z. T., P. A. De Troch, F. P. (1997). A method for retrieving soil moisture using active microwave data. *Physics and Chemistry of The Earth, 22*(3-4), 235-239.

Thoma, D., Moran, S., & Bryant, R. (2008). Appropriate scale of soil moisture retrieval from high resolution radar imagery for bare and minimally vegetated soils. *Remote Sensing of Environment, 112*(2), 403-414.

Tsan, M., Schmugge, T. J., & Jackson, T. J. (1984). Calculations of radar backscattering coefficient of vegetation-covered soils. *Remote Sensing of Environment, 15*(2), 119-133.

Ulaby, F. T. (1981). Microwave response of vegetation. *Advances in Space Research, 1*(10), 55-70.

Ulaby, F. T., Dubois, P. C., & van Zyl, J. (1996). Radar mapping of surface soil moisture. *Journal of Hydrology, 184*(1-2), 57-84.

Van der Velde, R., Zhongbo Su, & Yaoming Ma. (2008). Impact of Soil Moisture Dynamics on ASAR σ Signatures and Its Spatial Variability Observed over the Tibetan Plateau. *IEEE Transactions on geoscience and remote sensing, 9*(8), 5479-5491.

Wagner, W., Lemoine, G., Borgeaud, M., & Rott, H. (1999). A study of vegetation cover effects on ERS scatterometer data. *Geoscience and Remote Sensing, IEEE Transactions on, 37*(2), 938-948.

Wang, J. R., Shiue, J. C., Schmugge, T. J., & Engman, E. T. (1989). Mapping surface soil moisture with L-band radiometric measurements. *Remote Sensing of Environment, 27*(3), 305-311.

Wegmüller, U. (1990). The effect of freezing and thawing on the microwave signatures of bare soil. *Remote Sensing of Environment, 33*(2), 123-135.

Yisok, O., Jin-Young, H., & Seung-Gun, J. (2007, 11-14 Dec. 2007). *Retrieval of Soil Moisture and Surface Roughness from Backscatter Measurements of Vegetation Canopy.* Paper presented at the Microwave Conference, 2007. APMC 2007. Asia-Pacific.

Zhang, T., Wen, J., Su, Z., Velde, R. v. d., Timmermans, J., Liu, R., et al. (2009). Soil moisture mapping over the Chinese Loess Plateau using ENVISAT/ASAR data. *Advances in Space Research, 43*(7), 1111-1117.

Zribi, M., Le Hégarat-Mascle, S., Ottlé, C., Kammoun, B., & Guerin, C. (2003). Surface soil moisture estimation from the synergistic use of the (multi-incidence and multi-resolution) active microwave ERS Wind Scatterometer and SAR data. *Remote Sensing of Environment, 86*(1), 30-41.

APPENDIX - LIST OF TABLES

Appendix-Table 1 Soil moisture stations site description

Station ID	Lat/Lon	Elevation (m)	Topography	Land Cover	Soil type	OMC (g/kg)
CST_01	33°53'14.16" 102°08'25.62"	3431	River valley	Grass	NA	NA
CST_02	33°40'42.60" 102°08'18.66"	3449	River valley	Grass	NA	NA
CST_03	33°54'17.82" 101°58'15.66"	3507	Hill valley	Grass	NA	NA
CST_04	33°46'12.84" 101°43'52.98"	3504	Hill valley	Grass	NA	NA
CST_05	33°40'46.50" 101°53'21.78"	3542	Hill valley	Grass	NA	NA
NST_01	33°53'22.68" 102°08'27.48"	3431	River valley	Grass	Silt loam	18.37
NST_02	33°53'04.74" 102°08'32.28"	3434	River valley	Grass	Silt loam	18.37
NST_03	33°46'00.54" 102°08'50.52"	3513	Hill slope	Grass	Silt loam	49.11
NST_04	33°37'52.14" 102°03'25.56"	3448	River valley	Wetland	Silt loam	229.07
NST_05	33°38'05.10" 102°03'34.68"	3476	Hill slope	Grass	Silt loam	22.53
NST_06	34°00'29.70" 102°16'53.58"	3428	River valley	Grass	Silt loam	22.68
NST_07	33°59'13.74" 102°21'37.20"	3430	River valley	Grass	Silt loam	22.68
NST_08	33°58'19.44" 102°36'31.08"	3473	valley	Grass	Silt loam	33.76
NST_09	33°54'38.64" 102°33'00.78"	3434	River valley	Grass	Sandy loam	16.99
NST_10	33°51'07.74" 102°34'25.44"	3512	Hill slope	Grass	Loam-silt	24.19
NST_11	33°41'33.18" 102°28'36.12"	3442	River valley	Wetland	Silt loam	135.74
NST_12	33°37'16.02" 102°28'00.36"	3441	River valley	Grass	Silt loam	38.62
NST_13	34°01'53.70" 101°56'31.44"	3519	valley	Grass	Silt loam	28.58
NST_14	33°55'35.64" 102°07'42.78"	3432	River valley	Grass	Silt loam	29.58
NST_15	33°51'26.10" 101°53'28.08"	3752	Hill slope	Grass	Silt loam	56.08

APPENDIX - LIST OF TABLES

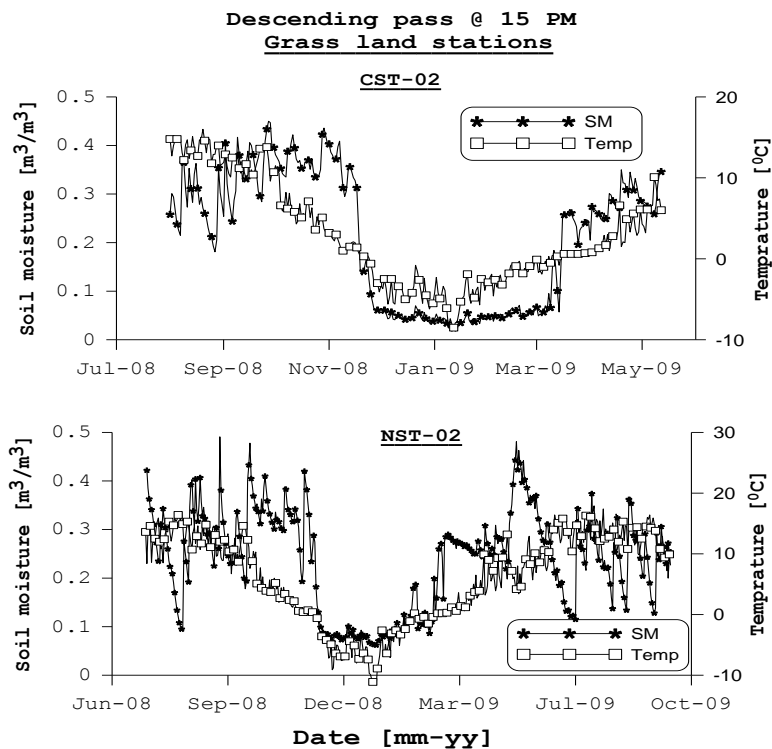**Appendix-Table 2 List of ASAR WSM observation over the study area in 2008**

Year	2008		
No of image	Accusation date	Pass	Polarization
1	9-Jan-08	Descending	VV
2	25-Jan-08	Descending	HH
3	29-Feb-08	Descending	HH
4	13-Jun-08	Descending	HH
5	2-Jul-08	Descending	HH
6	7-Jul-08	Ascending	VV
7	8-Jul-08	Descending	VV
8	18-Jul-08	Descending	VV
9	12-Aug-08	Descending	HH
10	31-Aug-08	Descending	VV
11	12-Sep-08	Ascending	VV
12	26-Sep-08	Descending	VV
13	2-Oct-08	Descending	HH
14	23-Oct-08	Ascending	VV
15	25-Nov-08	Descending	HH
16	5-Dec-08	Descending	VV
17	14-Dec-08	Descending	VV

APPENDIX - LIST OF TABLES

Appendix-Table 3 List of ASAR WSM observation over the study area in 2009

| Year	2009		
No of image	Accusation date	Pass	Polarization
1	1-Jan-09	Ascending	VV
2	18-Jan-09	Descending	VV
3	5-Feb-09	Ascending	VV
4	13-Feb-09	Descending	VV
5	22-Feb-09	Descending	VV
6	12-Mar-09	Ascending	VV
7	20-Mar-09	Descending	HH
8	29-Mar-09	Descending	VV
9	10-Apr-09	Ascending	VV
10	16-Apr-09	Ascending	VV
11	24-Apr-09	Descending	HH
12	3-May-09	Descending	VV
13	21-May-09	Ascending	VV
14	29-May-09	Descending	HH
15	7-Jun-09	Descending	VV
16	3-Jul-09	Descending	HH
17	30-Jul-09	Ascending	VV
18	29-Aug-09	Descending	HH
19	3-Sep-09	Ascending	VV
20	16-Sep-09	Ascending	HH
21	16-Oct-09	Descending	HH
22	25-Oct-09	Descending	VV
23	27-Oct-09	Ascending	VV
24	7-Nov-09	Descending	HH
25	17-Dec-09	Ascending	VV

Appendix-Figure 1 Soil moisture and temperature trend over grassland station on descending pass
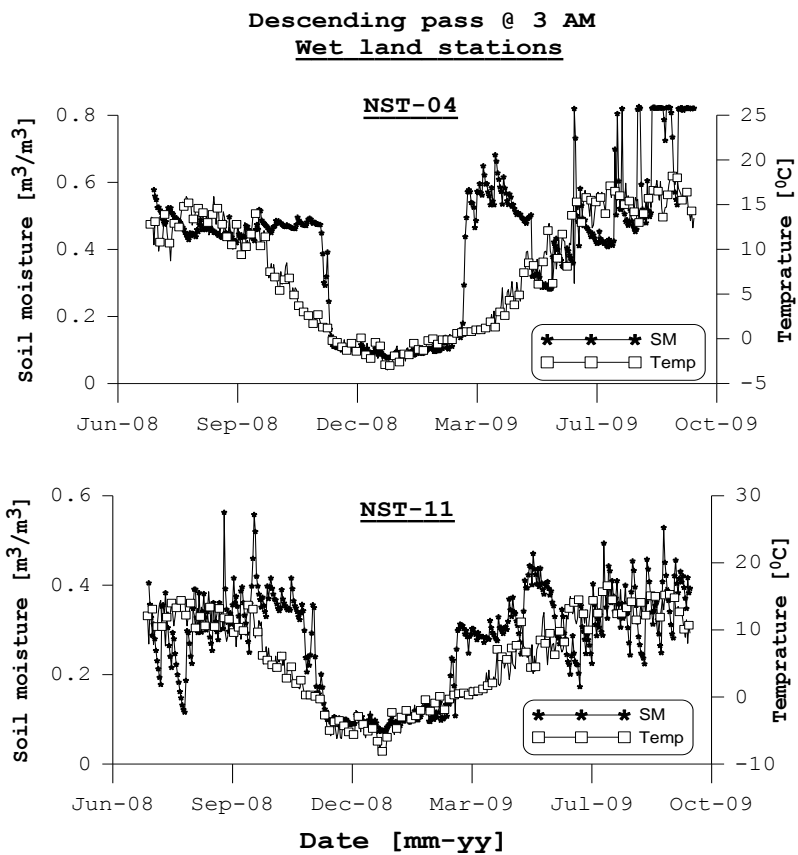
Appendix-Figure 2 Soil moisture and temperature trend over wetland station on descending pass

Descending pass @ 3 AM
Hill stations

NST-05

NST-15
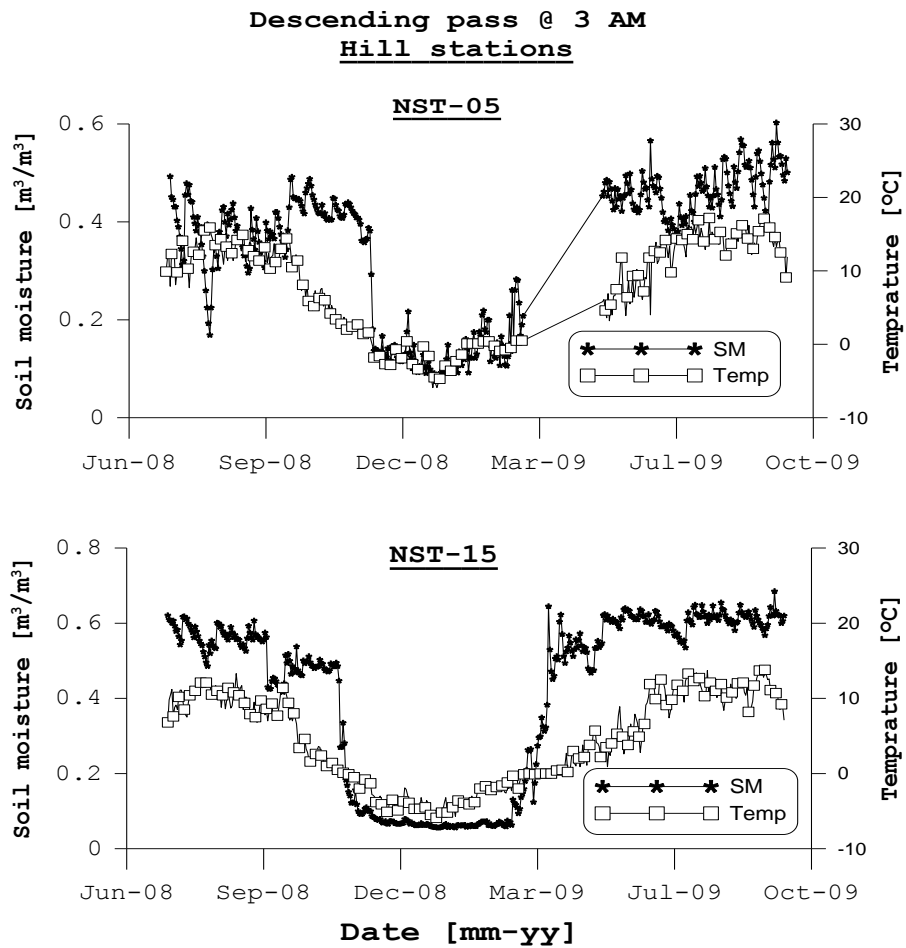
Appendix-Figure 3 Soil moisture and temperature trend over hill slope station on descending pass time